IMPROVING THE PERFORMANCE OF PEROVSKITE SOLAR CELLS FABRICATED IN AMBIENT ATMOSPHERE

A Thesis

by

NAGA ABHILASH CHADARAM

Submitted to the Graduate and Professional School of
Texas A&M University
in partial fulfillment of the requirements for the degree of

MASTERS OF SCIENCE

Chair of Committee,	Zi Jing Wong
Committee Members,	Xiaofeng Qian
	Pao Tai Lin
Head of Department,	Ibrahim Karaman

August 2021

Major Subject: Materials Science & Engineering

ABSTRACT

The metal halide perovskites have proven their potential in being the active absorption layer for the third-generation perovskite solar cells (PSCs). Their reported power conversion efficiency (PCE) is one of the fastest growths in the last decade, closing in towards the Shockley-Queisser limit and the silicon solar cell's highest recorded PCE. This was possible by exploiting properties, like tunable band gap, excellent photon absorption, and long carrier diffusion lengths. One of the possible ways to further improve the performance of the PSCs is by fabricating high-quality, defect-free perovskite films and optimizing the PSC's architecture accordingly. Ambient fabrication (Avg. 45% relative humidity) of PSCs usually causes non-uniform morphology and unequal crystal growth of the perovskite thin film leading to bad performance of the PSC. The motivation for this research is to fabricate high-efficiency metal halide perovskite solar cells with good optoelectronic and photovoltaic properties in complete ambient conditions i.e., without the use of an inert gas environment/glove box. Fabrication in such an environment leads to the formation of larger grains and defects. Hence, optimizing the fabrication process to minimize the defects, results in uniform deposition of perovskite active layer with larger grain size, which will aid in faster carrier transportation. By fine-tuning the growth conditions of every layer in the PSC and optimizing their fabrication variables, one can achieve improved performance from a PSC. Hence, choosing the most effective source materials and deposition conditions that work in ambient conditions for both electron transport layer (ETL) and hole transport layer (HTL) and optimizing the thin films for best extraction and transportation of charge carriers while also blocking the opposite charge carrier is essential. We took measures to improve the quality of the perovskite active layer by using mixed anti-solvent to increase the grain size and depositing a

passivation layer on perovskite thin film before the HTL to lower the surface defects. Therefore, a synergistic effect from various individual optimizations done at each layer and interface level was anticipated, which successfully improved the PCE of our PSCs fabricated in ambient conditions from around 7% to above 15%.

ACKNOWLEDGEMENTS

I would like to thank my committee chair, Dr. Zi Jing Wong, for his guidance and motivation, and my committee members, Dr. Xiaofeng Qian, Dr. Pao Tai Lin, for their support throughout the course of this research.

I would like to thank my lab mates Mr. Jinze Cai, Mr. Jitesh Pandya, Mr. Yixin Chen, Mr. Ziwei Fan, and Mr. Victor Vogt for their help towards my research work during my time in the lab.

Special thanks to Ms. Erin Bandza, for helping and guiding me through my graduate degree.

Thanks also go to my friends and colleagues and the department faculty and staff for making my time at Texas A&M University a great experience.

Finally, thanks to my mother and father for their moral, emotional, and financial support.

CONTRIBUTORS AND FUNDING SOURCES

Contributors

This work was supervised by a thesis committee consisting of Professor Zi Jing Wong of the Department of Aerospace engineering and Professor Xiaofeng Qian of the Department of Materials science and engineering and Professor Pao Tai Lin of the Department of Electrical and computer engineering.

The XRD data analyzed was provided by Dr. Nattamai Bhuvanesh. The SEM and AFM analyses presented were conducted in part by Mr. Ziwei Fan and Mr.Yixin Chen of the Department of Aerospace engineering.

All other work conducted for the thesis (or) dissertation was completed by the student independently.

Funding Sources

Graduate study was supported by a fellowship from the department of Materials science and engineering (MSEN) at Texas A&M University.

This work was also made possible in part by the President's Excellence Fund (X-Grant) and TAMU Start-up Fund.

NOMENCLATURE

PSC	Perovskite solar cell
PCE	Power conversion efficiency
RH	Relative humidity
ETL	Electron transport layer
HTL	Hole transport layer
CdTe	Cadmium telluride
CIGS	Copper indium gallium selenide
ITO	Indium doped tin oxide
V_{oc}	Open-circuit voltage
J_{sc}	Short-circuit current density
FF	Fill factor
TCO	Transparent conducting electrode
FTO	Fluorine doped tin oxide
RMS	Root mean square
HOMO	Highest occupied molecular orbitals
LUMO	Lowest unoccupied molecular orbitals
UV-VIS	Ultraviolet-visible
PTFE	Polytetrafluoroethylene
SEM	Scanning electron microscopy
PL	Photoluminescence
AFM	Atomic force microscopy
XRD	X-ray diffraction

TABLE OF CONTENTS

LIST OF FIGURES

1. INTRODUCTION

With the rapid growth of renewable energy usage around the globe with a major emphasis on solar energy, there has never been a harder push from the industry for innovative solutions to improve solar cell technology and reduce its costs to make it more affordable. This is where perovskite-based solar cells come in, by having a potential for high efficiency at a lower processing cost, they proved themselves as a worthy competitor for traditional silicon-based solar cells and other proven thin-film technologies like CdTe and CIGS [6]. From just under 4% efficiency a decade ago, they have currently achieved around 25% efficiencies nearing their practical limits [1-3]. But most of these PSCs are fabricated in controlled and inert atmospheres in glove boxes maintained at <1% moisture and O_2 [7-11], which is not a scalable process. Many research groups have been trying to fabricate high-efficiency PSCs in ambient conditions, but as of now, the PCE is still relatively low [4,5,12,13], and these PSCs also are susceptible to adverse effects of humidity and O_2 in the ambient conditions. Despite these hurdles, this is one of the most promising fields in both materials science and the solar energy industry.

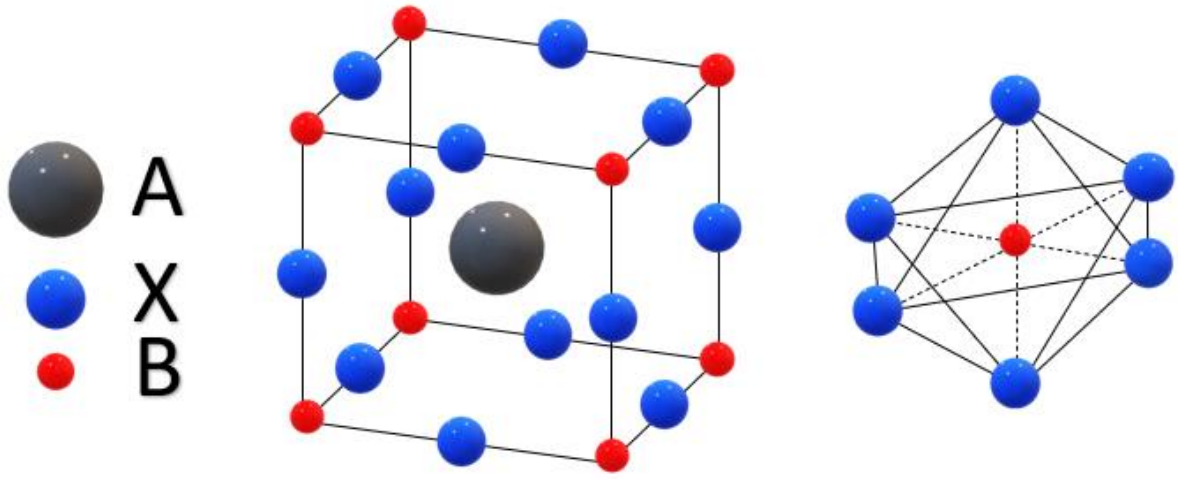

Fig. 1. ABX_3 perovskite structure with larger A cation occupied in the cubooctahedral site and BX_6 octahedron structure.

Perovskites have the general formula of ABX_3, where A and B represent cations where monovalent A (Organic- methylammonium (MA), formamidinium (FA), etc. or inorganic- Cesium (Cs), Rb (Rubidium), etc.) is bigger than divalent B (Lead (Pb), Tin (Sn), etc.), and X is usually a halogen like Chlorine (Cl), bromine (Br) and iodine (I). Cation A coordinates with 12 X anions and cation B coordinates with 6 X anions forming a cuboctahedral geometry and octahedral geometry, respectively as in Fig. 1. In ideal case scenarios, perovskites should possess a cubic structure with an octahedral network of BX_6 in the corners with cation A occupying the cuboctahedral voids. The BX_6 octahedral network highly influences the characteristics like bandgap and phase transition [14]. The tendency to form the perovskite structures is estimated by using the Goldschmidt tolerance factor (t) which is given by:

$$t = (R_A+R_X)/1.414(R_B+R_X)$$

Assuming the bond lengths are the algebraic sum of the ionic radii of the participating elements. Here R_A, R_B, R_X are the ionic radii of A, B, X, respectively. The value of t for a stable perovskite crystal structure is 0.88 to 1.1, and in most common cases it is almost 1. An Octahedral factor (μ) is another key factor for evaluating the stability of the perovskite crystal structure. A stable octahedron can be formed only if the value of μ is between 0.45 to 0.89 [15]. Where Octahedral factor (μ) is given by:

$$\mu = R_B/R_X$$

The perovskite structures have lower exciton binding energy, high dielectric constant, long-range charge transportation (100nm to even more than 1μm) [16]. These also possess very good photoelectric properties, and due to relatively cheaper raw material, low-temperature solution processability, and relatively easy synthesis, perovskite has been an excellent choice for an active layer for 3D planar heterojunction solar cells applications [17]. These features result in perovskite

solar cells with a high open-circuit voltage (V_{oc}) and a short-circuit current density (J_{sc}). The perovskite thin-film absorbs photons to produce excitons (electron-hole pairs) when exposed to sunlight as in Fig. 2. Free electron-hole pairs are generated because of the difference in exciton binding energy of the perovskite materials, they can either recombine back into excitons or generate a current. A standard and model perovskite material like Methylammonium lead triiodide ($MAPbI_3$)(with unit cell parameter of 6.27A^o and direct bandgap of 1.57V) [18] has high carrier mobility and longer lifetime, at least 100 nm of carrier diffusion distance, and low carrier recombination probability which results in high performing perovskite solar cells. These free charge carriers are transported to their respective transport layers and the electrons are collected by the Indium doped tin oxide (ITO) layer and the holes are collected at the metal electrode layer. And when a circuit is established between ITO and the metal electrode, photocurrent is generated in the external circuit.

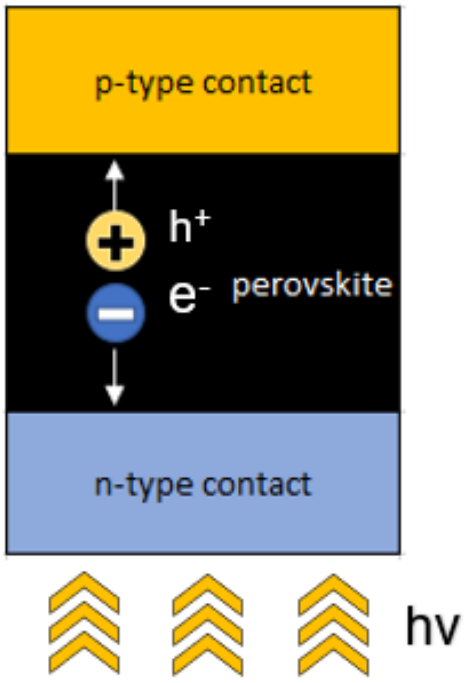

Fig. 2. Functioning mechanism of perovskite solar cells.

2. LITERATURE REVIEW

2.1 Planar n-i-p Heterojunction Architecture

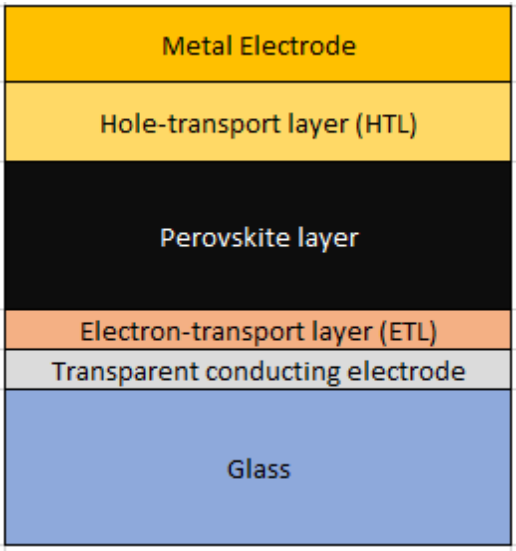

Fig. 3. Architecture of planar n-i-p heterojunction PSC.

The typical planar architecture of perovskite solar cells is depicted in Fig. 3. The system has a transparent conducting oxide (TCO) as an anode, n-type electron transport layer (Tin oxide (SnO_2) in our case), an intrinsic active layer of perovskite, p-type hole transport layer (Spiro-OMeTAD in our case), and Gold (Au) metal as cathode. Two interfaces are created between the perovskite and the carrier transport layers. Numerous works on the planar heterojunction perovskite solar cell architecture resulted in the precise understanding of the mechanism of photocurrent generation, which helped in optimizing the device down to each layer and successfully fabricating PSCs with high PCE. Snaith et al. introduced the planar heterojunction architecture in 2012, using $MAPbI_{3-x}Cl_x$ active perovskite layer and FTO/TiO_2/$MAPbI_2Cl$/Spiro-OMeTAD/Ag structure. But because of bad film coverage, the device could only achieve 1.8% PCE [19]. Upon optimizing the process, in 2013, Snaith et al. proposed a dual-source co-evaporation of MAI and $PbCl_2$ and deposited $MAPbI_{3-x}Cl_x$ absorber layer on c-TiO_2 ETL and could achieve a PCE of 15% with open-circuit

voltage (Voc) = 1.07v, fill factor (FF) = 67%, short circuit current (Jsc) = 21.5 mA/cm^2 [20]. In 2018, Dong Yang et al. and his team proposed a planar architecture with ethylene diamine tetra-acetic acid (EDTA) complexed SnO_2 as the ETL and Spiro-OMeTAD as the HTL, sandwiching the $FAPbI_3$ active perovskite layer with a trace amount of CS doped. They could achieve a highly efficient PSC with a champion PCE of 21.6% and Voc = 1.11v, FF = 79.2%, Jsc = 24.55 mA/cm^2 [21]. Even the latest certified record of 25.2% PCE made by Jeong, J., Kim, M., Seo, J. et al. in 2021, used a planar architecture by eliminating the major lattice defects in $FAPbI_3$ perovskite films by utilizing $HCOO^-$ anions [22]. Hence, the relative ease of fabrication and the functionality made the planar n-i-p heterojunction architecture a go-to option.

2.2 Indium Doped Tin Oxide Substrate

The ITO-coated glass substrate is depicted in Fig. 4. With a thickness of 100 nm, a measured sheet resistance of 20 Ω/sq., and a root mean square (RMS) roughness of 1.8 nm [23]. Despite having lower optical transparency and lower thermal stability than FTO, we still prefer ITO because of its superior electrical properties and a smoother finish as a TCO layer.

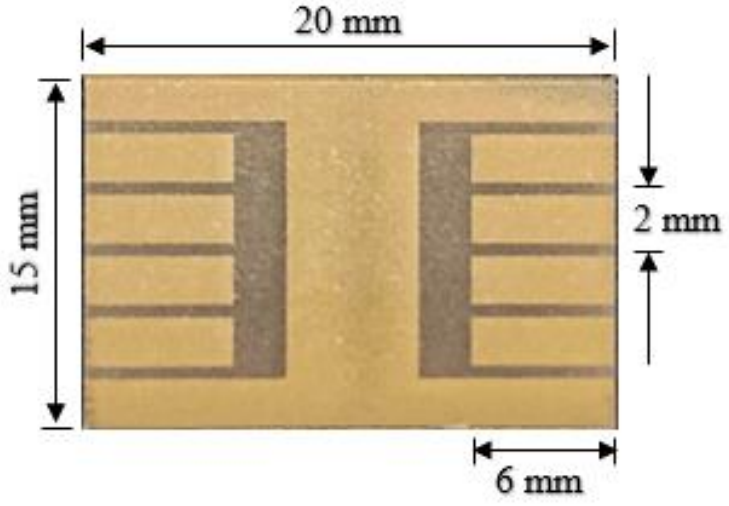

Fig. 4. Schematic of ITO substrate.

2.3 Electron Transport Layer

The primary function of an ETL is to efficiently extract and transport the photo-generated electrons to the anode by forming an electron-selective contact with the perovskite active layer, therefore blocking the migration of holes to the anode. This enhances the carrier separation and inhibits the charge recombination. ETLs should pose a very high transmittance in the UV-VIS region to maximize the solar spectrum's photon transmission. It should have high thermal stability, high charge mobility, minimal defect states, and have its HOMO and LUMO levels aligned according to the perovskite active layer used. The Dye-sensitized solar cells (DSSCs) heavily used TiO_2 as their ETL, hence TiO_2 became a widely adopted ETL even in the perovskite solar cell community. However, TiO_2 has its drawbacks of stability as an ETL for PSCs and the processing of TiO_2 needs high-temperature sintering for elongated time, making it incompatible with large-scale manufacturing at low costs. The conduction band minimum of $MAPbI_3$ is below that of TiO_2, which results in inefficient electron extraction. The photocatalytic effect of TiO_2 results in degradation of itself and the perovskite layer, especially when exposed to ultraviolet (UV) light for an elongated duration. Oxygen vacancy defect trap states in TiO_2 catalyze the non-radiative losses deteriorating the device performance. Such limitations forced the perovskite solar cell research community into searching for alternative ETLs [24]. Snaith et al. and co-workers used Al_2O_3 instead of TiO_2 and concluded that it enhanced the stability of the PSC to a great extent [25]. Kelly et al. and co-workers experimented with ZnO, which was commonly used as ETL for organic solar cells and had the advantage of being processed at low temperatures with environmentally safe solvents like water. But hydroxyl groups quickly degraded the PSCs, making ZnO a non-worthy competitor [26]. Further research was carried with ZnO [26-28], $ZnSO_4$ [29,30], WO_3 [31,32], In_2O_3 [33], $SrTiO_3$ [34], $BaSnO_3$ [35,36] etc. SnO_2 was the clear winner among them all

with high bulk carrier mobility (240 $cm^2 V^{-1} s^{-1}$) which is almost two orders higher than TiO_2, superior chemical stability, resistance to UV spectrum resulting in lower photocatalytic activity than TiO_2, more compatible energy band alignment with perovskite layer leading to minimal open-circuit voltage losses, better transmittance in UV-VIS spectrum. It also has a large bandgap of -3.6ev to -4ev compared to -3ev of TiO_2 [37], SnO_2 is air-stable, commercially available at low costs, and is also commercially processed at low cost due to low-temperature requirements. Ke et al. first used SnO_2 thin film as an ETL in regular planar-type PSCs and achieved a 16.02% PCE [38]. Later Jiang et al. synthesized the SnO_2 nanoparticles as the ETL and reported a 19.9% certified efficiency with very low hysteresis [39]. Hence, SnO_2 is one of the most promising ETLs, which contributed to a high recorded PCE of 23.32% for planar heterojunction PSCs [39]. The rate of electron transfer from the perovskite active layer depends on the ETL used in the PSC, as they all have different work functions. But it has been observed that Voc>1V for all TiO_2, SnO_2, and ZnO ETLs, reflecting that, unlike Jsc and FF, the Voc of the PSC does not depend on the energy level of the ETL [40].

2.4 Perovskite Active Layer

As mentioned above, perovskites are of ABX_3 configuration. The primary function of a perovskite active layer is to absorb the photons from the sunlight and generate electron-hole pairs for them to be transported towards the electrodes by the carrier transport layers. Kojima et al. fabricated a methylammonium lead triiodide ($CH_3NH_3PbI_3$) based PSC and achieved a PCE of 3.8% in 2009 [1] and this initiated extensive research on perovskite active layers in solar cells.

Methylammonium lead triiodide ($MAPbI_3$) based PSCs achieved a PCE up to 20% [41-46]. As stated previously, $MAPbI_3$ has a direct bandgap of around 1.57ev and hence has an absorption

spectrum of up to 800nm. It also has very low exciton binding energy (<10meV), a high absorption coefficient, charge-carrier mobilities, carrier diffusion lengths (>1μm), and a very low non-radiative recombination, which makes it a worthy candidate for PSC fabrication [1, 47-52]. But it is thermally unstable, hence the industry advanced to mixed cation perovskites ($MA_xFA_{1-x}PbI_3$) [53] mixed halide perovskites ($MAPbI_{2/3}Br_{1/3}$) [54], and a synergistic mixture of these two like $MA_xFA_{1-x}PbBr_{2/3}I_{1/3}$ [55]. All these changes are to fine-tune the bandgap and to use a broader spectrum of sunlight for energy conversion and fine-tune the optoelectronic properties.

2.5 Hole Transport Layer

Irrespective of the device architecture, HTL is a key element in fabricating an efficient and stable PSC. The primary function of HTL is to efficiently extract and transport photo-generated holes to the metal cathode by forming a hole-selective contact with the perovskite active layer, therefore blocking the migration of electrons to the cathode. Hence, this also enhances the carrier separation and inhibits the charge recombination. HTL should also have high thermal stability, high charge mobility, minimal defect states, and have its HOMO and LUMO levels aligned according to the perovskite active layer used. The transport layers should be thermally stable and resistive to external degrading factors. There can be organic and inorganic HTLs, for example, Spiro-OMeTAD, PTAA, NiO, CuO, Cu_2O, etc. In DSSCs, liquid redox electrolytes were used [56], but Bach et al. used a solid-state-based amorphous HTL called 2,2′,7,7′-tetrakis- (N, N-di-4-methoxyphenylamino) -9,9′-spirobifluorene (spiro-OMeTAD) [57]. The replacement of liquid electrolytes with solid-state HTL Spiro-OMeTAD, had proven to improve the effective PCE and stability even without encapsulation [57]. Spiro-OMeTAD has a plethora of advantages like a simplistic recipe, high melting point, solid state-amorphous, good conductivity, solution

processability, non-volatile, and does not react with perovskites [58]. This also has its HOMO and LUMO levels aligned to be compatible with most perovskite active layers. All these factors made it one of the most famous HTL for PSCs [58]. It has been giving consistent results since 1997 when it was first used as HTL [59]. Even the latest breakthrough of PSC with 25.2% PCE was fabricated with Spiro-OMeTAD [22].

2.6 Gold (Au) vs Silver (Ag) Top Electrode

The silver (Ag) electrode layer is deposited with a thickness of 100 nm, almost negligible resistance when compared to the complete cell, very high electrical conductivity, good reflectivity, and suitable work function for collection of holes [60]. Christian Wehrenfennig et al. and team in 2013 have first used Ag electrode in a planar $MAPbX_3$ PSCs, later it became a common electrode for minimizing the cost of fabrication of PSCs [61]. We in our research deposited Ag electrodes using Electron beam deposition in the initial architectures to test out the functioning of the device. Gold (Au) despite having lower electrical conductivity and charge carrier mobility, is preferred over Ag as an electrode for PSCs because of its chemical inertness. Unlike Ag, Au does not readily form any metal oxide/sulfide films on its surface, which reduces the effective conductivity, hence increasing the stability and lifetime of PSCs with Au top metal electrode. Hence in later part of this research we moved from Ag to Au as the preferred choice of electrode.

2.7 Ambient Fabrication of Perovskite Solar Cells

The fabrication conditions are of extreme importance when fabricating PSCs as they influence the quality and stability of the final perovskite thin films deposited. Hence, ambient fabrication as opposed to using an N_2 glove box will make our experiments susceptible to oxidation, effects of

humidity, any other contaminants/trace elements. The affect of humidity is predominant and occurs as per the equation below.

$$CH_3NH_3PbI_3 \xleftrightarrow{H_2O} CH_3NH_3I + PbI_2$$

The fabrication conditions can determine the crystal structure, composition, surface finish/morphology, optoelectrical properties of the perovskite thin film. But the advantages of the perovskite solar cells motivated for designing a facile fabrication method that is inexpensive and effective in producing high efficiency PSCs. Steady progress has been seen in the ambient-atmosphere fabrication, but the PCE in most cases is still lower than those fabricated in a controlled inert environment. In our research study, an attempt was made to optimize the fabrication conditions and the fabrication process itself at multiple layers and interfaces according to the ambient conditions, and a synergistic improvement in PCE has been observed from 7% to above 15%. This shows that upon further experimentation with better materials and further fine-tuning, higher efficiency PSCs can be fabricated in an ambient atmosphere with ease.

It has been explained why SnO_2 is a better choice for ETL in a previous section, the functioning of ETL also depends upon its source material. SnO_2 can be prepared by the sol-gel method by dissolving $SnCl_2$ in ethanol. Even though $SnCl_2$ is readily soluble in ethanol, it still benefits from longer stirring times for producing a better-performing film. Another source for SnO_2 is from SnO_2 colloidal solution in DI water. The ETL formed from this source is proven to produce PSCs with over 20% PCE [51,52]. This SnO2 film has a carrier mobility of 1.9×10^{-3} cm^2 $V^{-1}s^{-1}$, better compared to SnO_2 from $SnCl_2$ in ethanol. This ETL is further enhanced by complexing the SnO_2 with a chelating agent EDTA. This EDTA reacts with Sn^{+4} ions to form a stable and water-soluble complex. One primary advantage this has over SnO_2 is that there is an improved open-circuit voltage due to better band alignment of the EDTA-SnO_2 complex with the conduction band of the

$MAPbI_3$. And the electron mobility of this ETL is about three times that of SnO_2 [21]. EDTA is a chelating agent, makes the SnO_2 layer more hydrophilic upon complexing. This reduces the contact angle between the perovskite precursor and ETL surface and lowers the Gibbs free energy for the nucleation of perovskite crystals [21]. This results in a perovskite film of relatively higher quality and uniformity. But because of the scale and sensitivity of the particles, it was predominantly used in glove box fabrication of PSCs with a concentration of 2.67 wt.% [62,63]. We, as well as some research groups, attempted ambient fabrication at this concentration, but the reproducibility of uniformity of thin film was very bad. But as this is an aqueous solution, it is expected to be much resistant to the humidity in the ambient environment compared to other ETLs.

Fumin Li et al. and the team subjected the samples with SnO_2 layer to UV-Ozone treatment [64] and were heated to high temperatures around 200^0C before the single-step spin coating of the perovskite precursor. This supposedly eliminated the need for post-annealing of the perovskite film, but this experiment did not involve an anti-solvent treatment [49,50]. The $MAPbI_3$ precursor is supposed to be stirred before deposition, as PbI2 is not readily soluble in the solvent. Pronounced improvement in film uniformity and quality is observed when the precursor is stirred at an increment of 2 hours from 2 to 12 hours and deposited in the ambient atmosphere after filtering using a 0.45µm PTFE filter. But the humidity and O_2 in the ambient environment act as trap states and causes surface defects. This carrier transportation is hindered by surface defects. Anti-solvent is a solvent in which the targeted compound is less soluble, hence it causes precipitation when added to the solution in another solvent and helps in crystallization. Hence, using anti-solvent, one can enhance the surface morphology and optoelectronic and photovoltaic properties [65]. Many contrasting results have been published regarding which type of anti-solvent is the most effective, hence a better understanding of the anti-solvent's function and the mechanism is needed.

Anti-solvent-assisted ambient processes single-step spin coating method is one of the easiest and cost-effective ways of fabricating high-efficiency PSCs [65]. Xiao et al. in 2014, first experimented with anti-solvent assisted single step spin coating using chlorobenzene for controlled crystal growth of $MAPbI_3$ [66]. Another team used ether as an anti-solvent and achieved PCE ranging from 18.3-19.7% [67]. Usage of mixed anti-solvents in enhancing and regulating the crystal growth of perovskite active layers is uncommon. When choosing the constituents, it is essential to choose the anti-solvents with different evaporation rates and different solubilities from the perovskite active layer. Because of these differences, one anti-solvent dissolves the grain boundaries and evaporates, increasing the grain size, and the second anti-solvent re-dissolves the new grain boundaries and completely evaporates during the annealing process, resulting in even fewer grain boundaries i.e., larger grain size which results in easier carrier transportation which means higher efficiency PSCs with better optoelectronic properties [68]. Most anti-solvents are low-viscous liquids, and deposition by spin coating is affected by the glove box due to the restricted movement of the experimenter. Hence an ambient fabrication process alleviates this problem of human error.

Even though the surface is improved by mix anti-solvent treatment, the remaining defect states on the surface and in the grain boundaries act as target spots for oxygen and moisture. The non-radiative recombination taking place at ETL-perovskite and perovskite-HTL interfaces and on the grain boundaries of the perovskite thin film is a major deteriorating factor in achieving the theoretical efficiency limits for PSCs especially in ambient conditions [69-72]. A micro/nano outer coating is applied on the perovskite film as a protective passivating film to convert the active states to passive states. Lattice terminations of the perovskite along the crystal's surface, at interfaces, or misaligned grain boundaries are considered as active states along with unbonded metal sites or

halide vacancies. These active states create a potential difference and hence cause recombination [73,74]. Passivation is essential to mitigate the defects/trap states and establish an improved charge transfer between various functional layers of the PSC and improve the operational stability by inhibiting water to degrade the perovskite active layer [75].

In our research study, we attempt to analyze individual improvements from optimizing various layers and interfaces as mentioned above, and then a synergistic improvement is anticipated when all the optimizations are done in conjunction with ambient fabrication of PSCs. We diluted the concentration of SnO_2 from nanoparticle colloidal in DI water from 15 wt.% to 10 wt.% instead of 2.67 wt.%, which was mostly used in previous works [62,63,76,77] to synthesize EDTA-SnO_2 complex and achieve a uniform and reproducible coating and 10 wt.% is found to give a consistently uniform film. The SnO_2 coated samples are heated to 70^{o}C and maintained for 30 mins before the perovskite precursor deposition. This step aids in the process of perovskite crystallization. During the perovskite film deposition, we used the anti-solvent treatment with a mixed anti-solvent of 0.1% Isopropyl alcohol (IPA) in diethyl ether. Due to IPA having a higher vaporization temperature, it sutures the already formed grain boundaries to further increase the grain size and reduce surface irregularities like pinholes. We deposited a very thin film of trioctylphosphine oxide (TOPO) in chlorobenzene [78] for passivation of the perovskite surface before the deposition of HTL. Spiro-OMeTAD used as HTL was also stirred for 15 mins after synthesis to ensure complete dissolution of all the components in chlorobenzene and the static spin coating was done as opposed to dynamic spin coating, as the highest occupied molecular orbital (HOMO) energy level is lower and closer to perovskite in this route [79]. Improvements in film quality and/or device performance were observed with individual optimizations. But when we implemented them together a PSC with above 15% PCE was achieved.

3. EXPERIMENTATION

3.1 Single Step Perovskite Spin Coating

The schematic of the single-step spin coating process is depicted in Fig. 5. This is a solution-based fabrication method using the centrifugal force, specifically designed for low-cost thin-film deposition and it is one of the most used ambient fabrication methods for PSCs with high efficiencies. We followed a five-step process, which is, precursor deposition, spin acceleration, uniform angular velocity spin, spin deceleration, and evaporation throughout the process. Surface tension/wettability and viscosity of the precursor are the major factors determining the quality of deposition and the thickness of the film, along with the angular spin speed. Other factors which also affect the film thickness are the duration of spinning, the density of precursor, and the evaporation rates solutions used. Volatile components are uniformly evaporated during the process because of high angular spin speeds. We annealed the samples post-deposition of thin film, to evaporate the remaining solvent. We fabricated very thin uniform films with ease at relatively low costs, given the substrate size is small. As the size of the substrate increases, the fabrication parameters are harder to control. The material efficiency, though better than vapor-phase deposition, is still very low as only around 5% of the material remains in the final thin film. It is also highly dependent on the skill level of the researcher, and hence it is difficult to create multi-layered structures as we cannot guarantee a uniform and accurate deposition every time. The thin film quality can be easily affected by micro or nanoscale contaminants ranging from dust to humidity. The advantages overcome the disadvantages, hence for laboratory-scale experimentation, we have adopted the spin coating process for ambient fabrication of high-efficiency PSCs.

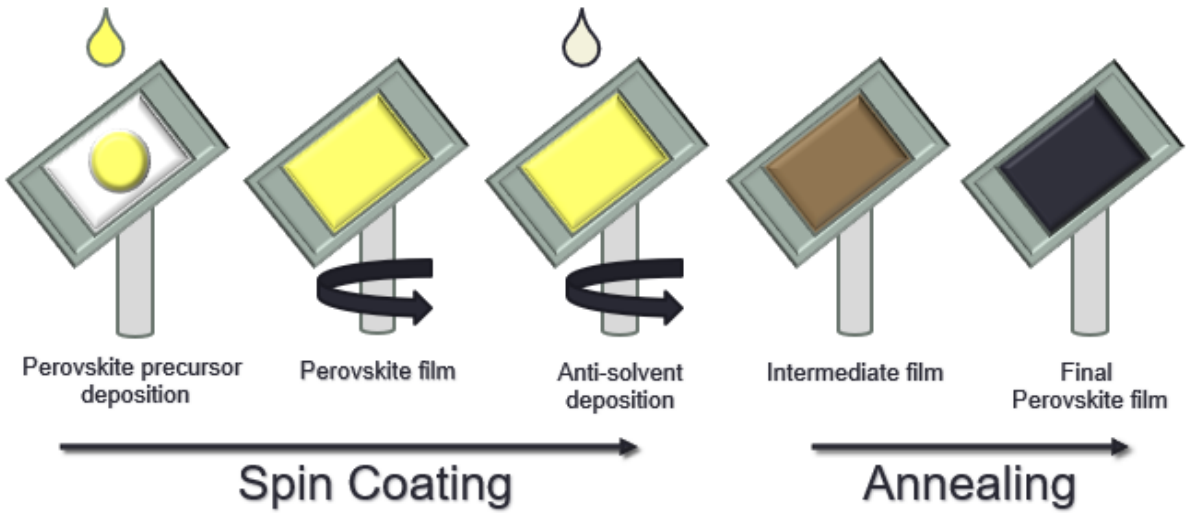

Fig. 5. Schematic of single-step spin coating with anti-solvent usage followed by annealing.

3.2 Materials

Substrate and cleaning: Indium-doped tin oxide (ITO) glass substrates (sheet resistance: 14–16 Ω/sq.) and Hellmanex™ III were purchased from Ossila, acetone, ethanol, isopropanol (IPA).

ETL: Tin (IV) oxide (15 wt.% in H_2O colloidal dispersion; SnO_2, Alfa Aesar), Ethylene diamine tetra-acetic acid (EDTA; >99.5%, Sigma-Aldrich), DI water

Perovskite: Anhydrous methylammonium iodide (MAI; >99%, Sigma-Aldrich), lead iodide (PbI2; 99.9985%, Alfa Aesar), anhydrous N, N-dimethyl formamide (DMF; 99.8%, Sigma-Aldrich), anhydrous dimethyl sulfoxide (DMSO; >99.9%, Sigma-Aldrich), anhydrous diethyl ether (DEE; >99.7%, Sigma-Aldrich), isopropanol (IPA).

Passivation: Trioctylphosphine oxide (TOPO; 99%, Sigma-Aldrich), chlorobenzene (>99%, VWR chemicals).

HTL: 2,2′,7,7′-tetrakis (N, N-di-p-methoxyphenyl amine)-9,9′-spirobifluorene (Spiro-OMeTAD; 99.0%, Sigma-Aldrich)

All these above-mentioned materials were used for the fabrication of different layers of the PSC.

3.3 Perovskite Solar Cell Fabrication Process

The planar heterojunction PSC architecture of the champion device fabricated in our study is ITO/EDTA-SnO_2/$MAPbI_3$/TOPO/Spiro-OMeTAD/Au. Sequential deposition of thin films on Glass/ITO substrate using spin coater is done. The ITO substrates are first cleaned by sonicating with detergent, IPA, and DI water for 15 mins each. We then dry them with pressurized air/N_2 and subject them to UV ozone treatment for 25 mins to eliminate any organic contaminants and improve the wettability of the substrate surface. These are then preheated at 70°C for 30 mins to remove any microscopic moisture. By dissolving 0.6 mg of EDTA in 1 ml of deionized water and diluting the 15 wt.% SnO_2 colloidal dispersion with deionized water to 10 wt.%. These two individual solutions are stirred at room temperature for 2 hours to ensure complete dissolution. These solutions are then mixed with a 1:1 volume ratio and stirred for 5 hours at 80°C. The ETL thin-film i.e., EDTA-SnO_2 is formed by spin coating the resulting solution at 5500 rpm for 30 secs. Samples are annealed at 180°C for 30-40 mins followed by 10 mins of UV ozone treatment. The SnO_2 coated samples are heated to 70°C. $MAPbI_3$ is made by dissolving 1:1 MAI and PbI_2 in a solution of dimethylformamide (DMF) and dimethyl sulfoxide (DMSO), stirring the precursor for at least 8-10 hours to ensure complete dissolution, filtered with 0.45µm PTFE filter to remove any undissolved PbI_2 and deposited over ETL using a single step spin coating method at 4000 rpm for 30 secs. We used a mixed-anti solvent of 0.1% IPA in di-ethyl ether and deposited it by dynamic spin coating during the perovskite thin film deposition step at the 10 secs mark. The samples are annealed at 65°C for 1 min and 100°C for 10 mins and a reflective mirror-like black perovskite film is observed (Fig. 11.). 2 mg of Tri-octyl phosphine oxide (TOPO) is dissolved in 1 ml of chlorobenzene (CB) and its thin film is used as a passivation layer deposited at 7000 rpm for 60 secs. The Spiro-OMeTAD is used as HTL, depositing at 4000 rpm for 30 secs (Fig. 18.). And

finally, gold (Au) electrode (Fig. 21.) of 100nm is deposited using the thermal evaporation process. This fabrication is done based on the energy band's structure diagram of all the thin films in PSC, depicted in Fig. 6.

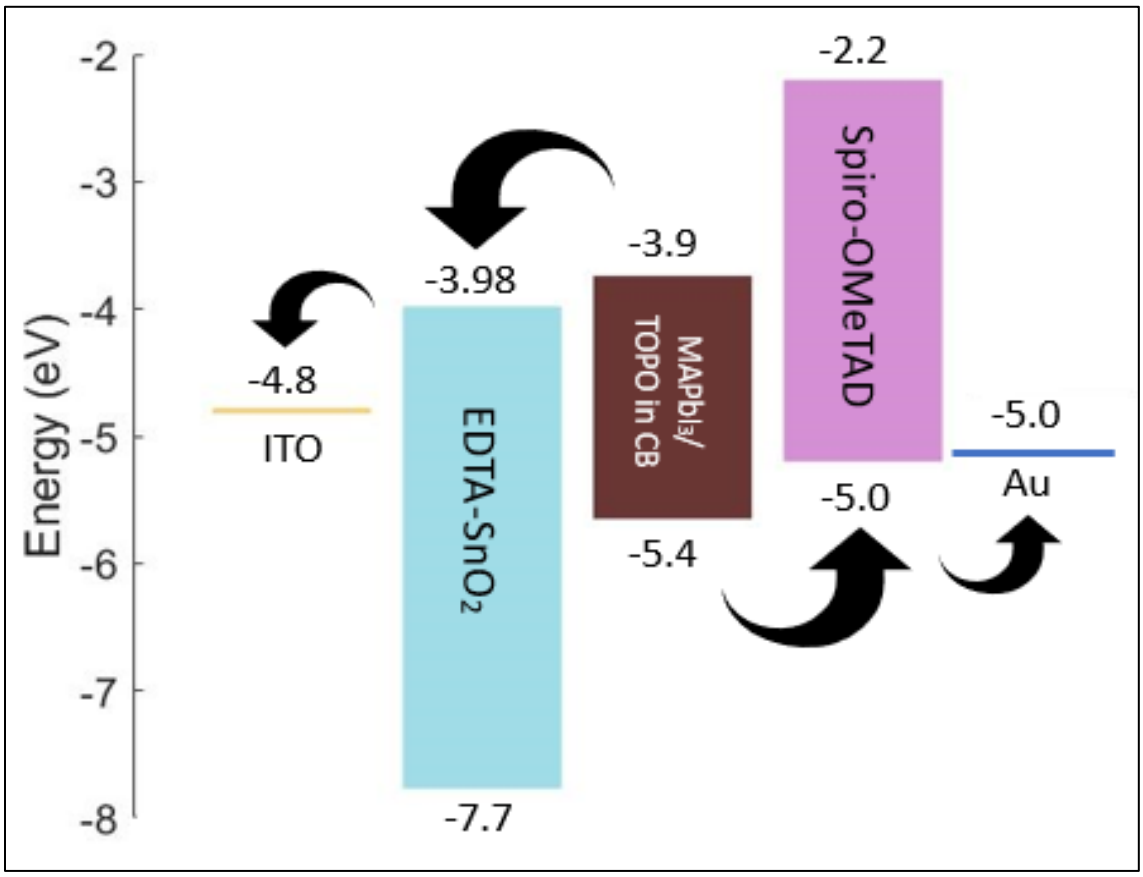

Fig. 6. Energy-band alignment diagram of final PSC architecture.

3.4 Characterization and Testing

Among the characterization methods of PSCs, we have done imaging using scanning electron microscopy (SEM) of different thin film surface morphologies (Fig. 10.) and the cross-section to verify the thickness of each thin film layer deposited (Fig. 8.) using the Tescan FERA-3 Model GMH Focused Ion Beam Microscope in the Materials characterization facility (MCF). Photoluminescence (PL) is tested for verifying the presence of characteristic peaks of the

perovskite material and the intensity peak change according to the ambient conditions (Fig. 16.) using the Olympus BX50 microscope with the help of the Mercury (Hg) lamp as the light source. Finally, the Jsc, Voc, FF, and PCE can be tested using the Newport solar simulator (1 sun equivalent intensity i.e., 100 mW/sq.cm) and solar cell I-V test system from Ossila to get the IV characteristics and the final PCE of the PSC (Fig. 23.). The surface roughness of the perovskite layer was measured by Bruker Dimension Icon AFM in the MCF (Fig. 9,15,19.). The phase purity of the nanocrystalline $MAPbI_3$ was analyzed by X-ray Diffraction (XRD) using Bruker-AXS D8 Advance ECO X-ray powder diffractometer using Cu Ka x-rays and a Pathfinder 0D detector in the chemistry department (Fig. 17.).

4. RESULTS AND DISCUSSION

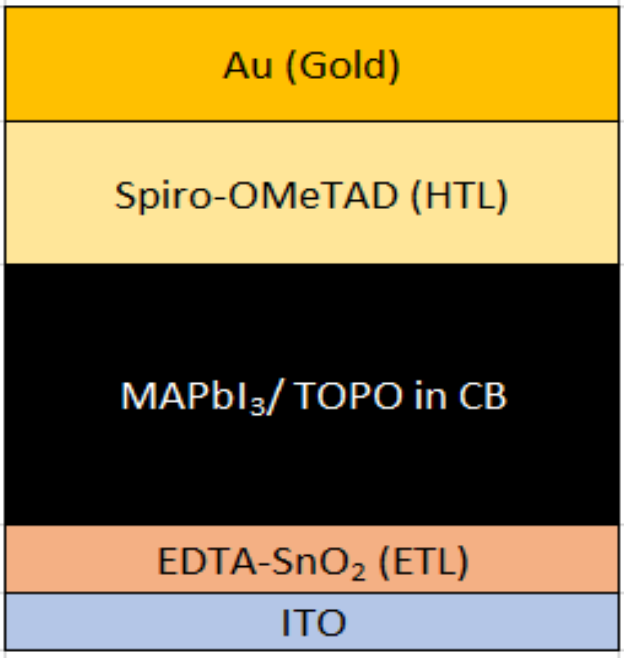

Fig. 7. Schematic of our PSC architecture.

The fabricated PSCs are based on the Fig. 7. architecture of multiple individual and blended layers. The basic substrate is ITO on glass. We deposit EDTA-SnO_2 as the ETL. $MAPbI_3$ is our choice of perovskite, and it is passivated with TOPO dissolved in chlorobenzene. Spiro-OMeTAD as HTL is deposited on top, followed by a 100 nm deposition of Au metal as the top electrode to complete the device architecture. Fig. 8. shows the cross-sectional SEM image of the final device architecture. We optimized this architecture to match the band structures of perovskite and the ETL and HTL and Au metal. This is done to make sure the ETL/Perovskite layer is transporting electrons to ITO and blocking holes, and similarly, HTL is transporting holes to Au and blocking electrons. This results in minimization of recombination of charge carriers, hence improving the FF and V_{oc}.

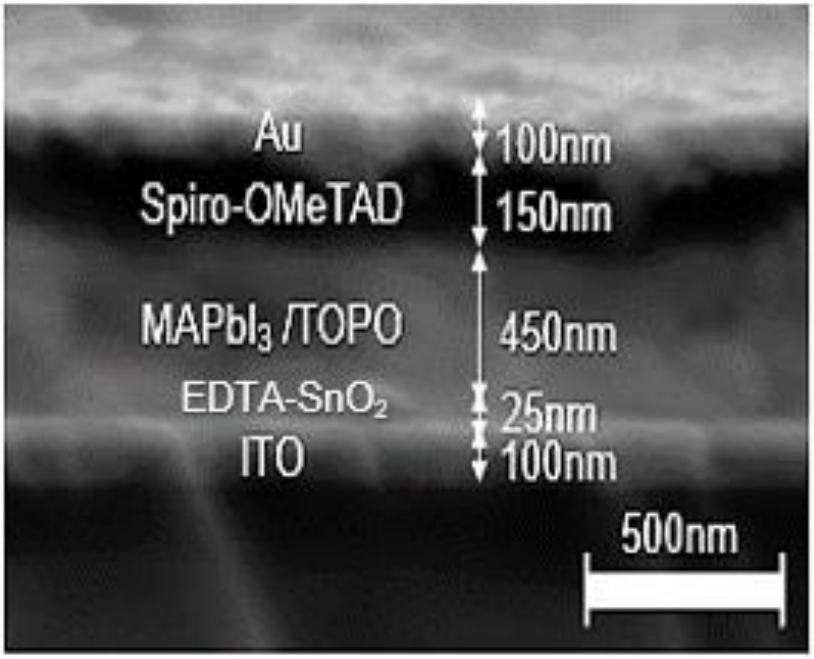

Fig. 8. Cross-sectional SEM image of our final PSC architecture.

4.1 Electron Transport Layer

EDTA-SnO_2 is our choice of ETL for our final architecture. EDTA is a chelating agent that forms a five-member ring structure with Sn^{+4} and is used to enhance the performance of SnO_2 as an ETL [21]. This solution was freshly prepared for most fabrications for uniform film coverage.

Atomic force microscopy (AFM) is performed with SnO_2 and EDTA-SnO_2 deposited on cleaned ITO substrates to check for the surface roughness as shown in Fig. 9. The results prove that EDTA-SnO_2 has a lower RMS roughness of 1.29 nm compared to the 1.31 nm of the SnO_2 layer. Lower roughness signifies lower surface irregularities and traps states. This helps in better film deposition in later stages of the architecture.

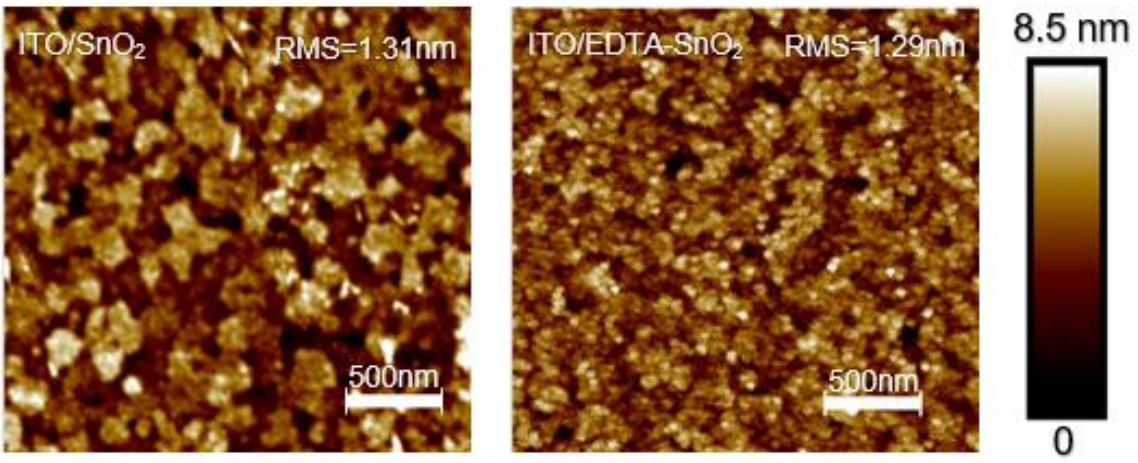

Fig. 9. AFM topographical images of SnO_2 and EDTA-SnO_2 on ITO substrates.

A reproducible high-quality perovskite thin film with good surface coverage and crystallinity is very essential for the good performance of the PSCs. We tested spin coating of $MAPbI_3$ onto both SnO_2 and EDTA-SnO_2 individually. And as per the literature review [21], we can observe that the perovskite film formed on EDTA-SnO_2 is more uniform and pin-hole free compares to that of SnO_2. The quality of the film is improved along with the average grain size. The average grain size of the perovskite film deposited on SnO_2 was 700 nm, but the average grain size of the perovskite film deposited on EDTA-SnO_2 was 780 nm. This increase in grain size is synonymous to lower grain boundaries i.e., lower surface defects which in turn mean improved charge carrier mobilities to the ITO electrode. This was possible because of the hydrophilic nature of the EDTA-SnO_2 thin film, which reduced the contact angle with the perovskite precursor. A lower contact angle of about 20.67^o helps lower the Gibbs free energy required for nucleation, helps in better wettability of the ETL-perovskite interface, and a lowered surface energy results in increased grain size of the perovskite crystal structure [21]. This can be observed in the SEM images in Fig. 10.

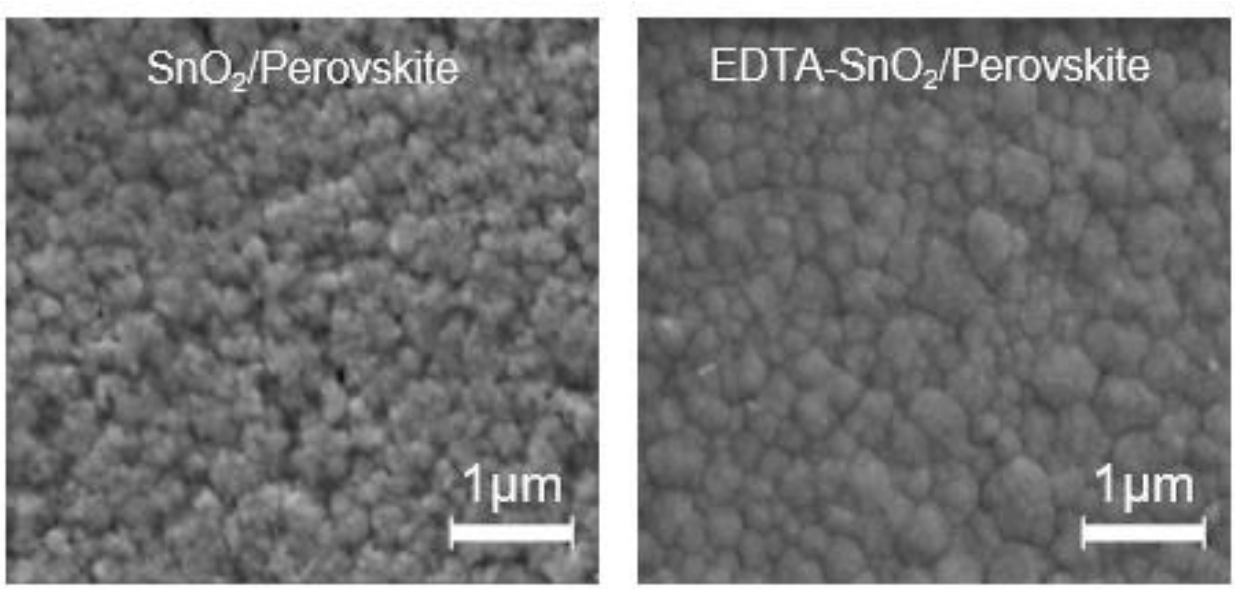

Fig. 10. SEM images of perovskite film morphology on different ETLs.

4.2 $MAPbI_3$ Perovskite Film

The reason behind choosing $MAPbI_3$ is that it is one of the most stable perovskite materials out there and hence it is extensively studied by researchers around the world. It has very good optoelectronic properties and has proven reproducibility of uniform perovskite films with good film coverage. This layer is the most adversely affected by the ambient conditions, is generally fabricated in controlled environments. The effect of moisture is very obviously seen during the ambient fabrication of the perovskite layer. In around 45% RH, and after optimizing all other fabrication parameters, we expect to get a thin film with a glossy black reflective finish as shown in the Fig. 11. This does not necessarily mean a high-performing device, but it is merely a visual proof of uniform thin film deposition with good crystallinity.

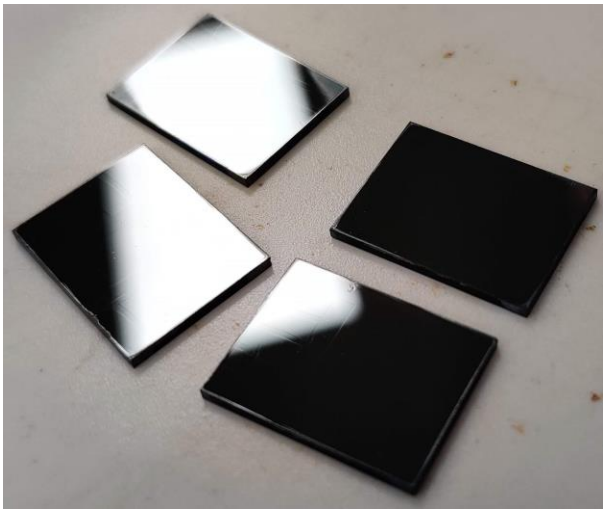

Fig. 11. $MAPbI_3$ thin film surface post-annealing.

To achieve this finish, we used the anti-solvent technique during the fabrication of the $MAPbI_3$ layer. The anti-solvent used is Di-ethyl ether. The solubility of $MAPbI_3$ is lower in di-ethyl ether than in DMF. Hence it causes the perovskite to precipitate and helps in crystallization. This anti-solvent technique is further enhanced by using a mixed anti-solvent. This has two solutions in which our targeted compound is less soluble than its actual solvent and one of them has a higher evaporation rate than the other. The mixed anti-solvent used here is 0.1% IPA in di-ethyl ether. This solution has very low viscosity and hence the usage of this can be better controlled in the ambient fabrication. The solvent with a lower evaporation rate re-dissolves the already formed grain boundaries and sutures them resulting in the formation of larger grains [68]. This increase in grain size is synonymous with lower grain boundaries, which are a form of surface defects. Hence having lower surface defects leads to better charge carrier transportation. The average grain size when we used just the di-ethyl ether was 590 nm, and when 0.1% IPA in di-ethyl ether was used, the average grain size increased to 700 nm, as seen in the Fig. 12.

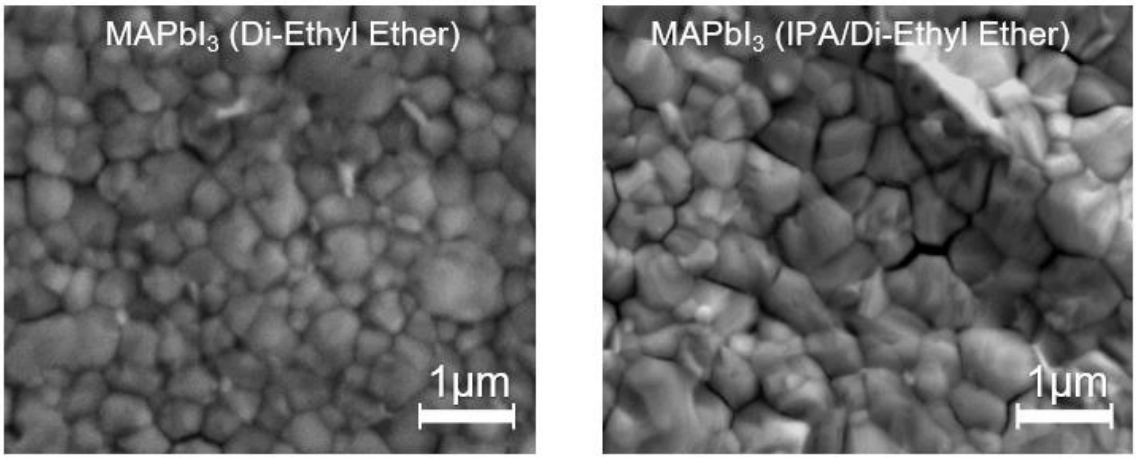

Fig. 12. SEM images of (Left) $MAPbI_3$ using normal anti-solvent with avg. grain size of 590 nm. (Right) $MAPbI_3$ using mixed anti-solvent with avg. grain size of 700 nm.

4.3 Passivation

2 mg of Tri-octyl phosphine oxide dissolved in 1 ml of chlorobenzene is used for the passivation of the perovskite layer. A very thin layer of passivation is deposited to not interfere with the optoelectronic functions of the PSC. The layer formed is so thin, the macro view of the surface is almost indistinguishable from the perovskite layer as seen in Fig. 13.

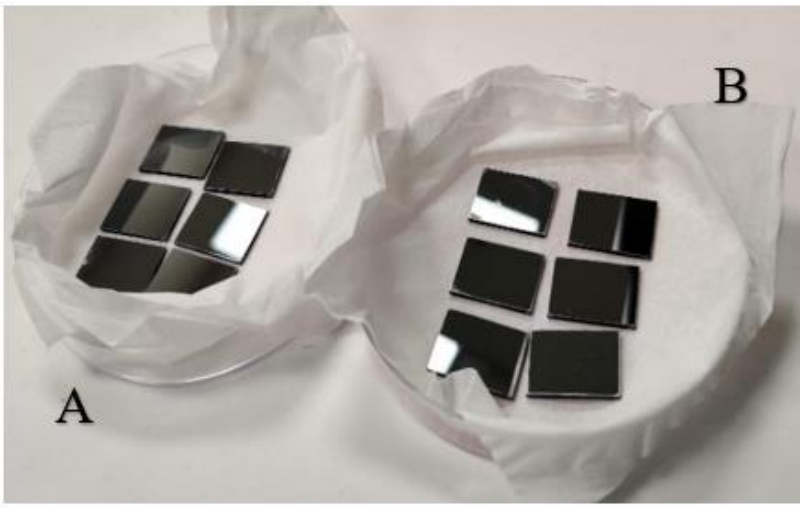

Fig. 13. Perovskite thin film (A) before passivation and (B) after passivation.

This method is predominantly used for passivating the surface and sub-surface defects and trap states to improve the surface finish and film quality as seen in Fig. 14. This also provides some level of protection from the deteriorating effects of moisture, resulting in longer retention of PL.

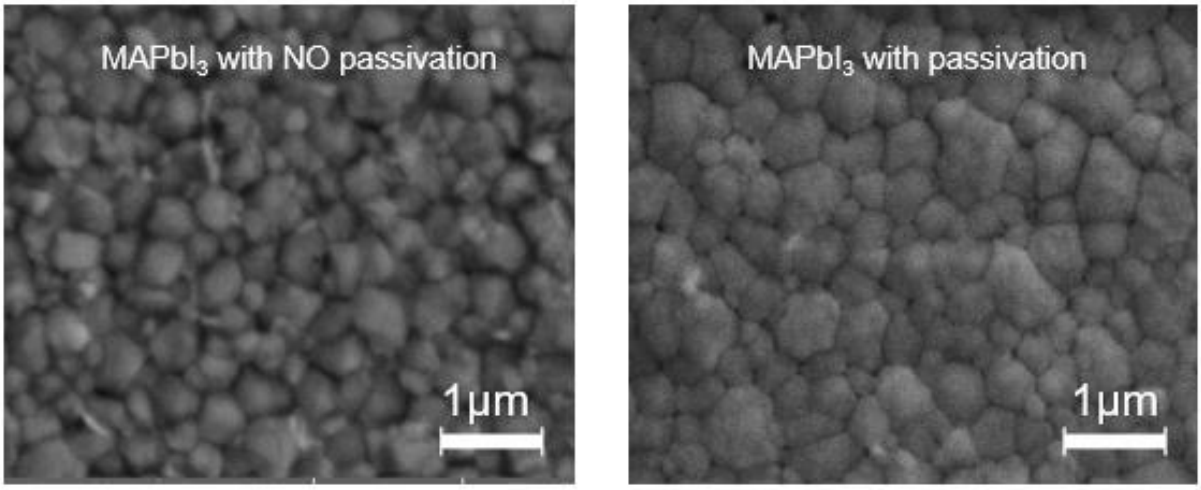

Fig. 14. Improvement in $MAPbI_3$ film quality before and after passivation.

AFM measurements are done before and after the passivation process to verify the improvement in surface finish and quality. The surface roughness of the perovskite film is decreased from a 29.1 nm to 11 nm RMS roughness as shown in Fig. 15. This decrease in roughness enables for a better deposition quality and adhesion of the HTL hence improving the performance of the total device.

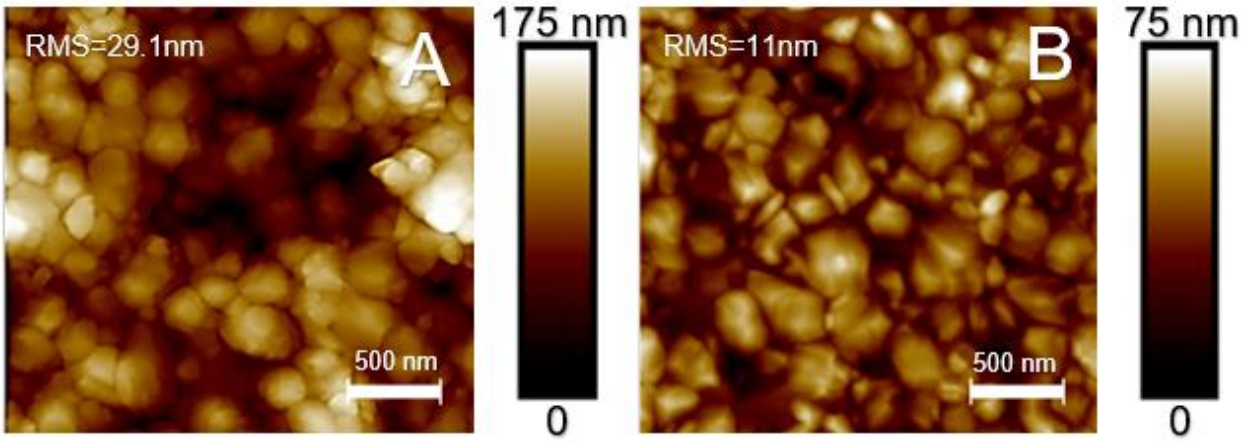

Fig. 15. AFM topography of perovskite layer (A) without any passivation, (B) after passivation.

Due to lower surface defects and trap states, a higher amount of charge carriers can be transported to the transport layers resulting in a slight improvement in the peak intensity during the photoluminescence (PL) measurements as seen in Fig. 16.

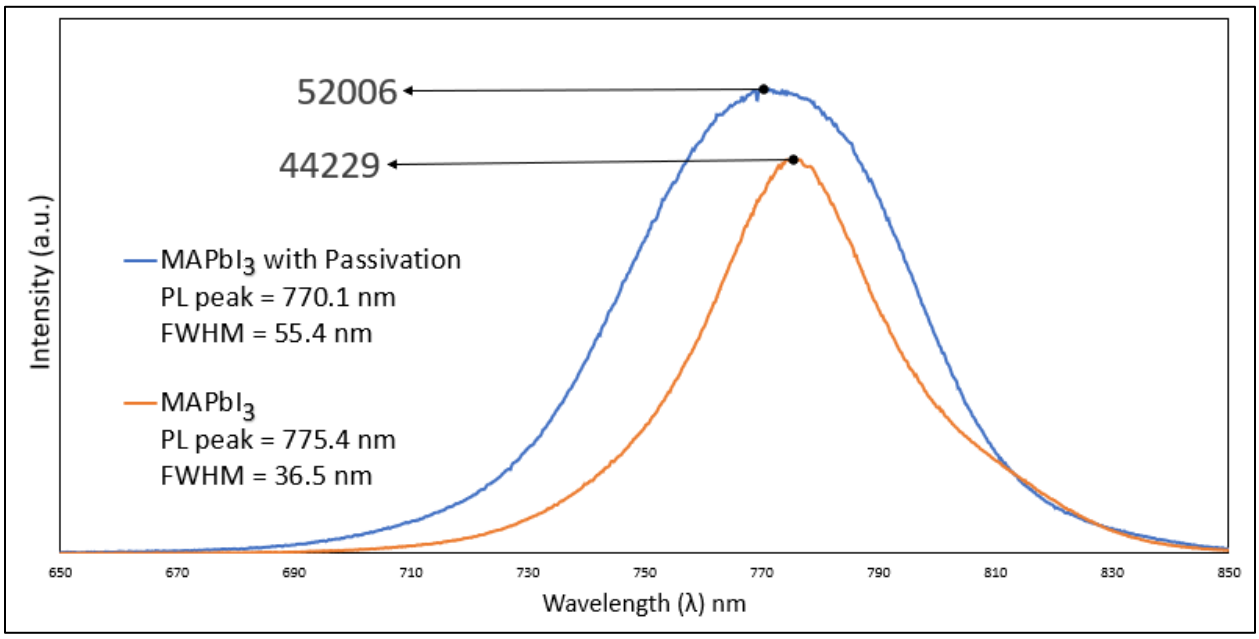

Fig. 16. Comparative PL performance before and after passivation of $MAPbI_3$.

Finally, XRD measurements were done before and after passivation to verify the existence of the α-phase of MAPbI3. The resulting graph was consistent with the literature review [80] meaning there are no unwanted phases or impurities present in the material. The XRD measurement of passivated perovskite film also shows almost the same peaks (Fig. 17.), indicating that the passivation is not causing any phase change and not hindering the optoelectronic functions of the perovskite film.

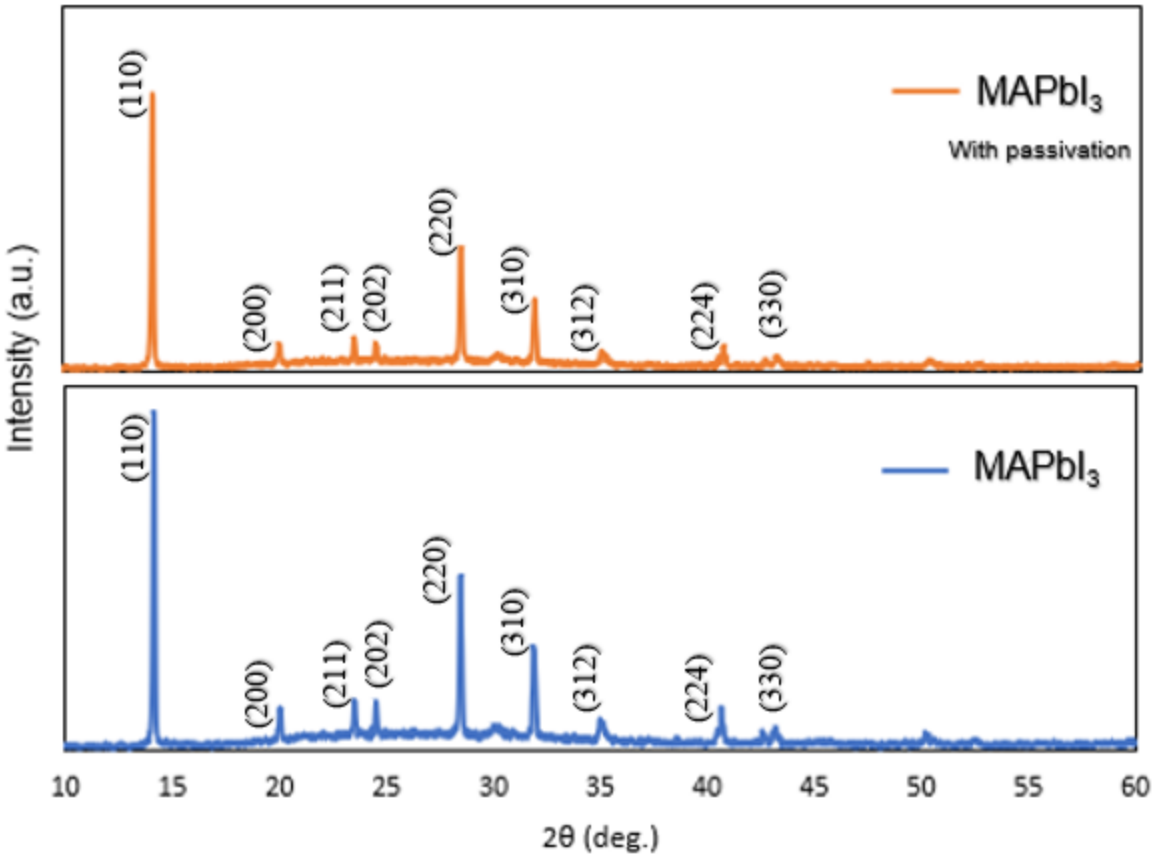

Fig. 17. XRD patterns of $MAPbI_3$ before and after passivation.

4.4 Hole Transport Layer

Spiro-OMeTAD has proven itself as one of the best HTLs out there for n-i-p architecture PSCs. But the necessary hygroscopic dopants in it like Lithium bis(trifluoromethanesulfonic)imide (LiTFSI) pose problem for the stability of the device [81]. In its pristine form, Spiro-OMeTAD suffers from low charge carrier mobilities. P-doping it to increase the hole conductivity is an essential step to improve its function as an HTL. This p-doping is achieved by oxidation of the Spiro-OMeTAD by placing the substrates in an oxygen environment for a certain time before final metal electrode deposition. Also, the pristine Spiro-OMeTAD absorbs photons in the UV spectrum, and upon sufficient oxidation, it displays strong absorption in the visible and near-

infrared spectrum. Hence oxidation of Spiro-OMeTAD is very essential for it to reach appreciable conductivity values. But despite the hurdles, it is still one of the most preferred HTL for PSCs. Another factor of differentiation of Spiro-OMeTAD is the way it is deposited onto the substrate. One being static spin coating in which the HTL is deposited on the stationary substrate, another is dynamic spin coating in which the HTL is deposited onto the substrate in rotation. These both produce different surface finishes as shown in Fig. 18. The static spin coating usually produces a more uniform finish whereas the dynamic spin coating results in a surface finish with multiple irregularities.

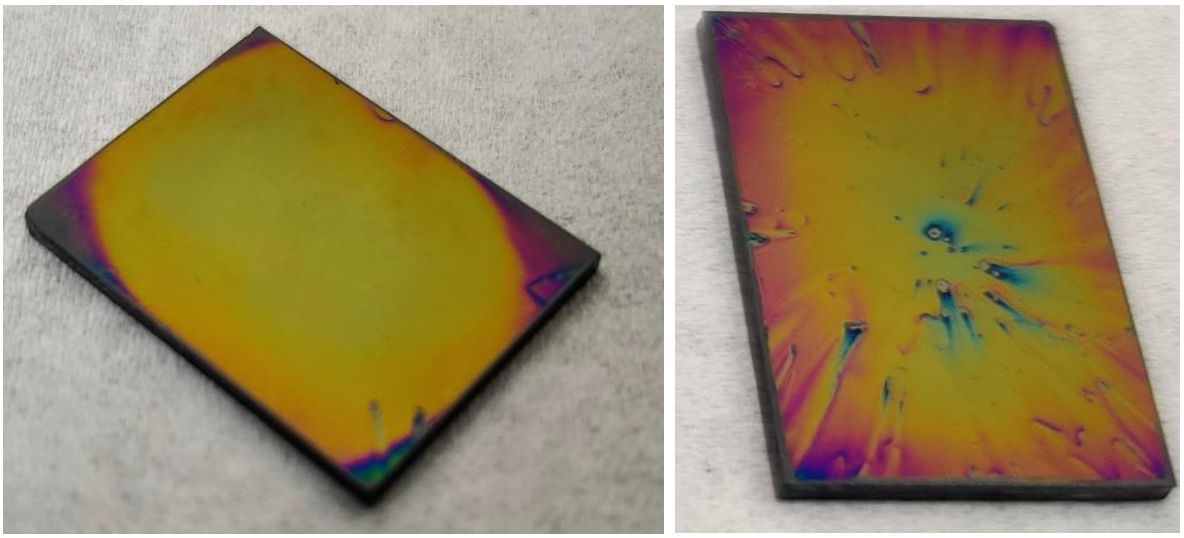

Fig. 18. (Left) Static spin coating and (right) dynamic spin coating of Spiro-OMeTAD.

AFM measurements are done for both static spin-coated and dynamic spin-coated Spiro-OMeTAD. As expected from the macroscopic surface finish, the static spin-coated samples are much smoother with RMS roughness of 14.4 nm, where are the dynamic spin-coated samples have an RMS roughness of 23.2 nm as shown in Fig. 19. The smoother the finish, the better interface is formed when the top electrode is deposited and lower is the chance for surface and sub-surface defects, which is essential for higher carrier charge transfer.

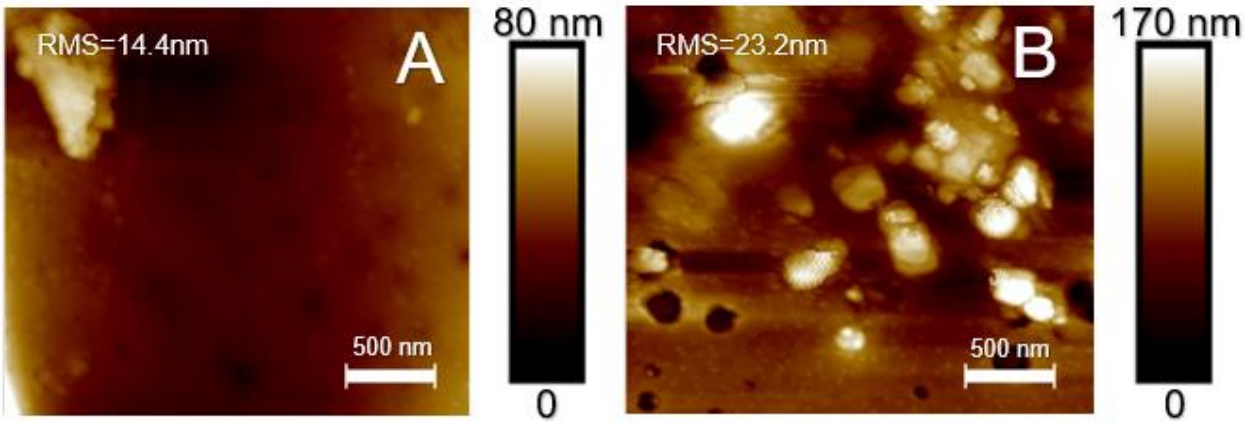

Fig. 19. AFM topography of (A) static; (B) dynamic spin-coated Spiro-OMeTAD.

Another major reason to prefer static spin-coating over dynamic spin-coating of Spiro-OMeTAD is that the static spin-coated layer is better aligned with the architecture of the PSC compared to the dynamic spin-coated layer. The HOMO level in this case is closer to both the perovskite and the Au top electrode as shown in the Fig. 6, 20., resulting in much higher and easier charge carrier mobility. Hence this plays a crucial role in the improvement of the performance of the PSC.

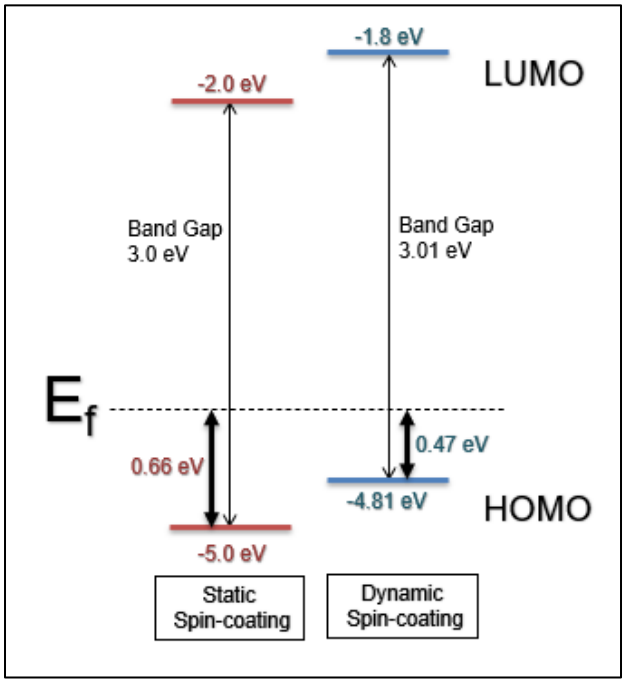

Fig. 20. Energy band diagram of Static vs Dynamic spin coating of Spiro-OMeTAD.

4.5 Gold (Au) vs Silver (Ag) Top Electrode

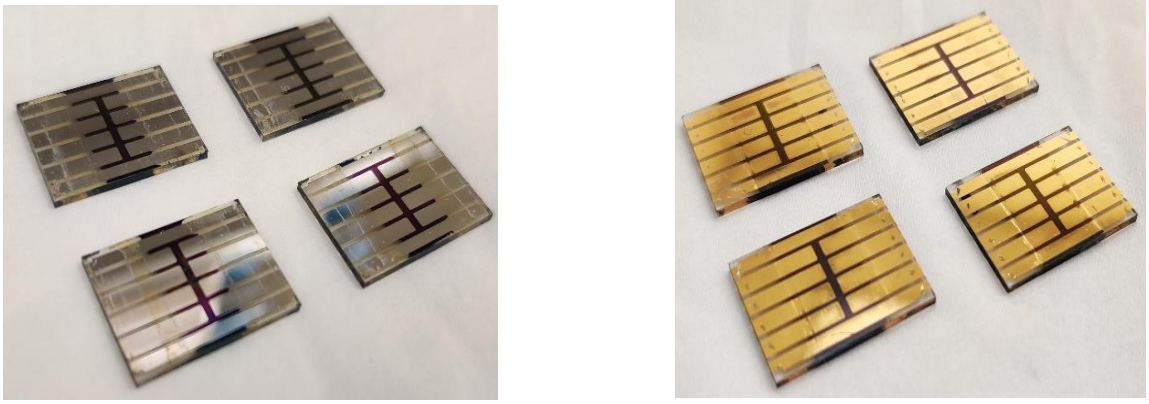

Fig. 21. Ag metal electrode (left); Au metal electrode (right) deposited samples.

We have fabricated samples with both Silver (Ag) and Gold (Au) top electrodes (Fig. 21.) Ag was preferred as a top electrode for minimizing the total cost of fabrication of the PSC. But using Ag comes with its own set of disadvantages. Ag having a higher affinity towards oxygen than Spiro-OMeTAD, it de-oxidizes the HTL, resulting in lower hole transport mobilities. Hence Au being much resistive to chemical interaction with oxygen results in proper better performing devices. Another disadvantage of Ag is that it turns yellow within a few weeks of device fabrication as shown in Fig. 22. This results in a drastic decrease in the performance of the device when compared to the Au electrode-based PSC stored for an equally long time under identical conditions. This color change is due to the formation of silver iodide, caused by the reaction between iodine in $MAPbI_3$ based perovskites [82]. This reaction is accelerated when the devices are exposed to an ambient atmosphere. The proposed mechanism is that methylammonium iodide (MAI) is transported through the pinholes in the Spiro-OMeTAD to the Ag electrode resulting in the formation of silver iodide [82,83]. Hence, we are made to choose the expensive Au as the top electrode for our PSCs due to its chemical inertness and because its work function is better aligned with the HTL's energy band levels resulting in much faster charge carrier mobility.

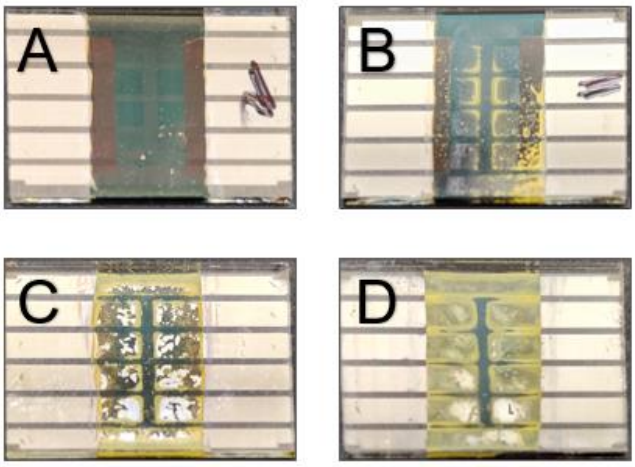

Fig. 22. (A) Freshly fabricated PSC (B) PSC after 7 days (C) PSC after 10 days (D) PSC after 14 days - Degradation of the PSCs due to silver-iodide formation.

4.6 Performance of PSCs

Incorporating all the above-mentioned optimizations at various layers and interfaces, a synergistic improvement in the performance of the perovskite solar cell is observed achieving a champion PCE of 15.37%. With a fill factor of 60.5%, short-circuit current density (J_{sc}) of 19.7 mA/cm^2 and an open circuit voltage (V_{oc}) of 1.03V. The I-V curve is shown in Fig. 23.

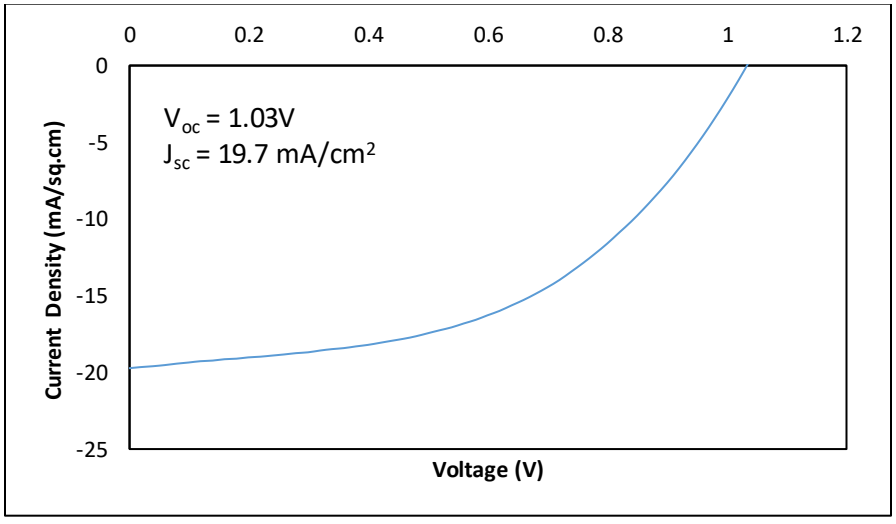

Fig. 23. IV characteristics of champion device of 15.37% PCE.

Using Au as the top electrode improved the reproducibility and life span of the PSCs. A very high percentage of devices were staying active even after repeated testing cycles spanning over multiple days with a relatively lower depreciation in PCE compared to Ag counterparts. The distribution of 120 devices fabricated with Au as electrode is shown in Fig. 24. with around 20 devices having more than 14% PCE. Hence, despite its high cost, usage of Au as top electrode gave consistently improved PCEs over Ag counterparts.

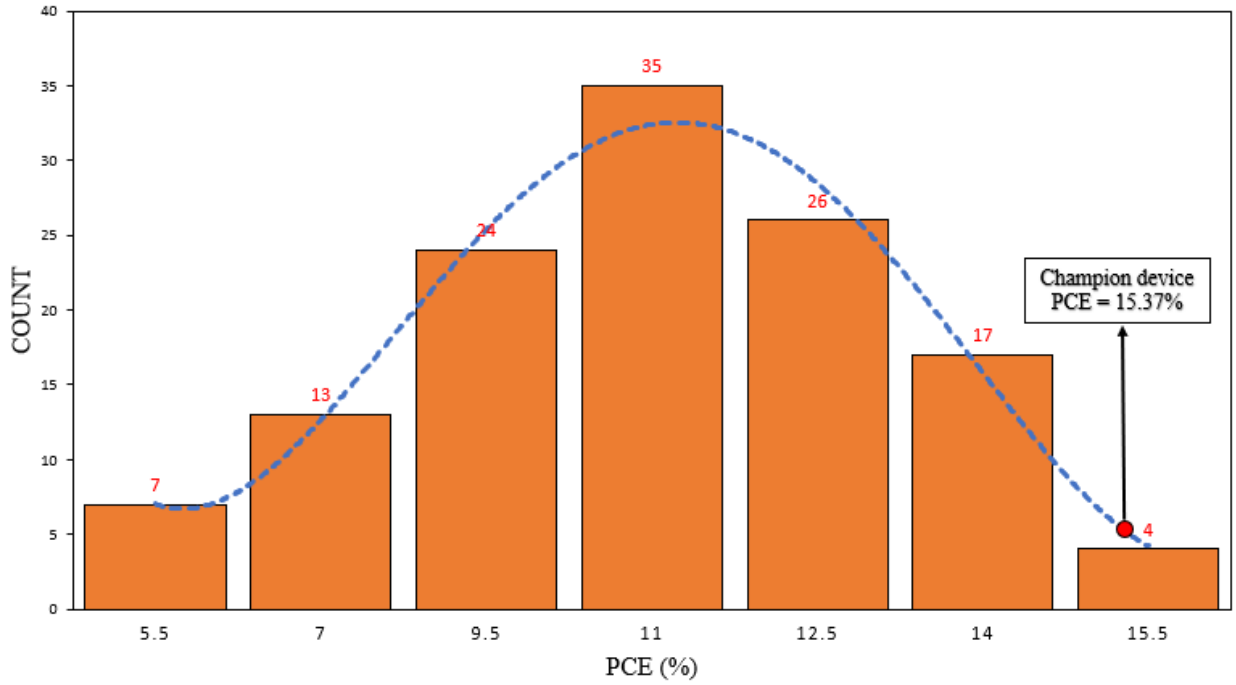

Fig. 24. Frequency distribution of PCE of 120 PSCs with Au top electrode.

5. CONCLUSION AND FUTURE SCOPE

This research study is an attempt to fabricate inexpensive and working organic-inorganic metal halide PSC with high power conversion efficiency and good IV characteristics in ambient conditions (Average 45% RH) to achieve a synergistic effect of multiple optimizations done at different thin-film interfaces and fabrication processes. From all the optimizations we attempted, we could achieve a champion device of 15.37% PCE. The deposition of gold (Au) as the top electrode enhanced the performance and stability of the devices significantly. The devices were functioning and active for relatively longer than when Ag was deposited as the top electrode.

As stated above ambient fabrication of PSCs is detrimental to the functioning of the device as it induces surface, sub-surface and internal defects and results in poor morphology as well as poor interface chemistry resulting in degradation of the PSC. This degradation of the device architecture negatively affects the overall performance of the device. One of the techniques to minimize the effect of ambient conditions on the device fabrication is pre-heating the substrates before ETL deposition, evaporating any microscopic moisture left on the surface after the cleaning process, and pre-heating the ETL deposited samples before perovskite deposition. Better crystallization due to faster evaporation of solvents was observed when these preheated samples were used for perovskite film deposition. The actual mechanism which facilitates better quality perovskite films due to preheating is still not completely understood and should be studied soon as it is proven to give consistent results.

Ambient fabrication of PSCs has come a long way in just a few years, now reaching PCEs above 20%. But certain limiting factors are to be addressed like new and novel materials like carbon-inks, carbon pastes, carbon nanotubes, and graphene to replace the current generation of HTLs which are usually hygroscopic and metal electrodes [84]. These opportunities must be rigorously

studied for fabricating high PCE PSCs in ambient environments. Ambient fabricated mixed-cation perovskites have better stability and performance. Recently an $FA_{1-x}MA_xPbI_3$ with PEAI passivation-based PSC achieved a PCE of 23.32% at 30-40% RH [39]. Also, mixed-cation mixed-halide perovskites are proven to have better stability than simpler perovskites. Hence, moving forward, these types of complex perovskites are to be focused upon for better performing PSCs. Simpler modifications like the addition of electron blocking layer and hole blocking layers in the architecture of the PSCs [85] might complicate the fabrication process and interface chemistry, but when optimized could result in a better performing device with almost negligible charge recombination. One other limiting factor of PSCs is their scalability due to the spin-coating fabrication method. Even though it is one of the best methods to produce high-efficiency PSCs in laboratory conditions, the performance of PSCs drops drastically with the increase in the size of the substrate. Therefore, despite all the achievement with the ambient fabrication of PSCs, there is much more untapped potential which could further enhance their performance.

REFERENCES

1. Kojima, A., Teshima, K., Shirai, Y., and Miyasaka, T. (2009). Organometal halide perovskites as visible-light sensitizers for photovoltaic cells. *Journal of the American Chemical Society*, *131*(17), 6050-6051.
2. See https://www.nrel.gov/pv/cell-efficiency.html for efficiencies of perovskite solar cells.
3. Huang, J., Yuan, Y., Shao, Y., and Yan, Y. (2017). Understanding the physical properties of hybrid perovskites for photovoltaic applications. *Nature Reviews Materials*, *2*(7), 1-19.
4. Eze, V. O., Seike, Y., and Mori, T. (2020). Synergistic Effect of Additive and Solvent Vapor Annealing on the Enhancement of MAPbI3 Perovskite Solar Cells Fabricated in Ambient Air. *ACS Applied Materials and Interfaces*, *12*(41), 46837-46845.
5. Parashar, M., Singh, R., and Shukla, V. K. (2021). Fabrication of perovskite solar cells in ambient conditions. *Materials Today: Proceedings*, *34*, 654-657.
6. Jena, A. K., Kulkarni, A., and Miyasaka, T. (2019). Halide perovskite photovoltaics: background, status, and future prospects. *Chemical reviews*, *119*(5), 3036-3103.
7. Eze, V. O., Lei, B., and Mori, T. (2016). Air-assisted flow and two-step spin-coating for highly efficient CH3NH3PbI3 perovskite solar cells. *Japanese Journal of Applied Physics*, *55*(2S), 02BF08.
8. Eze, V. O., and Mori, T. (2016). Enhanced photovoltaic performance of planar perovskite solar cells fabricated in ambient air by solvent annealing treatment method. *Japanese Journal of Applied Physics*, *55*(12), 122301.
9. Lei, B., Eze, V. O., and Mori, T. (2015). High-performance CH3NH3PbI3 perovskite solar cells fabricated under ambient conditions with high relative humidity. *Japanese Journal of Applied Physics*, *54*(10), 100305.

10. Patel, J. B., Wong-Leung, J., Van Reenen, S., Sakai, N., Wang, J. T. W., Parrott, E. S., ... and Johnston, M. B. (2017). Influence of interface morphology on hysteresis in vapor-deposited perovskite solar cells. *Advanced Electronic Materials*, *3*(2), 1600470.
11. Raga, S. R., Jung, M. C., Lee, M. V., Leyden, M. R., Kato, Y., and Qi, Y. (2015). Influence of air annealing on high efficiency planar structure perovskite solar cells. *Chemistry of Materials*, *27*(5), 1597-1603.
12. Wu, J., Dong, J. J., Chen, S. X., Hao, H. Y., Xing, J., and Liu, H. (2018). Fabrication of efficient organic-inorganic perovskite solar cells in ambient air. *Nanoscale research letters*, *13*(1), 1-7.
13. Wang, F., Zhongbiao, Y., Sarvari, H., Park, S., Graham, K., Zhao, Y., and Chen, Z. D. (2017, June). Fabrication of Efficient CH3NH3PbI3 Solar Cells in Ambient Air. In *2017 IEEE 44th Photovoltaic Specialist Conference (PVSC)* (pp. 1044-1047). IEEE.
14. Park, N. G. (2015). Perovskite solar cells: an emerging photovoltaic technology. *Materials today*, *18*(2), 65-72.
15. Tilley, R. J. (2016). *Perovskites: structure-property relationships*. John Wiley and Sons.
16. Zhou, D., Zhou, T., Tian, Y., Zhu, X., and Tu, Y. (2018). Perovskite-based solar cells: materials, methods, and future perspectives. *Journal of Nanomaterials*, *2018*.
17. Green, M. A., Ho-Baillie, A., and Snaith, H. J. (2014). The emergence of perovskite solar cells. *Nature photonics*, *8*(7), 506-514.
18. Li, C., Soh, K. C. K., and Wu, P. (2004). Formability of ABO3 perovskites. *Journal of alloys and compounds*, *372*(1-2), 40-48.
19. Qiu, J., Qiu, Y., Yan, K., Zhong, M., Mu, C., Yan, H., and Yang, S. (2013). All-solid-state hybrid solar cells based on a new organometal halide perovskite sensitizer and one-dimensional TiO 2 nanowire arrays. *Nanoscale*, *5*(8), 3245-3248.

20. Liu, M., Johnston, M. B., and Snaith, H. J. (2013). Efficient planar heterojunction perovskite solar cells by vapour deposition. *Nature*, *501*(7467), 395-398.
21. Yang, D., Yang, R., Wang, K., Wu, C., Zhu, X., Feng, J., ... and Liu, S. F. (2018). High efficiency planar-type perovskite solar cells with negligible hysteresis using EDTA-complexed SnO 2. *Nature communications*, *9*(1), 1-11.
22. Jeong, J., Kim, M., Seo, J., Lu, H., Ahlawat, P., Mishra, A., ... and Kim, J. Y. (2021). Pseudo-halide anion engineering for α-FAPbI 3 perovskite solar cells. *Nature*, 1-5.
23. See www.ossila.com/products/pv-substrates?variant=1200245025 for product data.
24. Leijtens, T., Eperon, G. E., Pathak, S., Abate, A., Lee, M. M., and Snaith, H. J. (2013). Overcoming ultraviolet light instability of sensitized TiO 2 with meso-superstructured organometal tri-halide perovskite solar cells. *Nature communications*, *4*(1), 1-8.
25. Tsutomu Miyasaka, & Takuro Murakami. (2012). High-efficiency hybrid solar cell using nano-superstructure of organometallic halide perovskite crystals. Science , 338(6107), 643-647.
26. Yang, J., Siempelkamp, B. D., Mosconi, E., De Angelis, F., and Kelly, T. L. (2015). Origin of the thermal instability in CH3NH3PbI3 thin films deposited on ZnO. *Chemistry of Materials*, *27*(12), 4229-4236.
27. Son, D. Y., Im, J. H., Kim, H. S., and Park, N. G. (2014). 11% efficient perovskite solar cell based on ZnO nanorods: an effective charge collection system. *The Journal of Physical Chemistry C*, *118*(30), 16567-16573.
28. Kim, J., Kim, G., Kim, T. K., Kwon, S., Back, H., Lee, J., ... and Lee, K. (2014). Efficient planar-heterojunction perovskite solar cells achieved via interfacial modification of a sol–gel ZnO electron collection layer. *Journal of Materials Chemistry A*, *2*(41), 17291-17296.

29. Yeom, E. J., Shin, S. S., Yang, W. S., Lee, S. J., Yin, W., Kim, D., ... and Seok, S. I. (2017). Controllable synthesis of single crystalline Sn-based oxides and their application in perovskite solar cells. *Journal of Materials Chemistry A*, *5*(1), 79-86.

30. Bera, A., Sheikh, A. D., Haque, M. A., Bose, R., Alarousu, E., Mohammed, O. F., and Wu, T. (2015). Fast crystallization and improved stability of perovskite solar cells with Zn2SnO4 electron transporting layer: interface matters. *ACS applied materials and interfaces*, *7*(51), 28404-28411.

31. Wang, K., Shi, Y., Dong, Q., Li, Y., Wang, S., Yu, X., ... and Ma, T. (2015). Low-temperature and solution-processed amorphous WO X as electron-selective layer for perovskite solar cells. *The journal of physical chemistry letters*, *6*(5), 755-759.

32. Zhang, J., Shi, C., Chen, J., Wang, Y., and Li, M. (2016). Preparation of ultra-thin and high-quality WO3 compact layers and comparision of WO3 and TiO2 compact layer thickness in planar perovskite solar cells. *Journal of Solid-State Chemistry*, *238*, 223-228.

33. Qin, M., Ma, J., Ke, W., Qin, P., Lei, H., Tao, H., ... and Fang, G. (2016). Perovskite solar cells based on low-temperature processed indium oxide electron selective layers. *ACS applied materials and interfaces*, *8*(13), 8460-8466.

34. Bera, A., Wu, K., Sheikh, A., Alarousu, E., Mohammed, O. F., and Wu, T. (2014). Perovskite oxide SrTiO3 as an efficient electron transporter for hybrid perovskite solar cells. *The Journal of Physical Chemistry C*, *118*(49), 28494-28501.

35. Shin, S. S., Yeom, E. J., Yang, W. S., Hur, S., Kim, M. G., Im, J., ... and Seok, S. I. (2017). Colloidally prepared La-doped BaSnO3 electrodes for efficient, photostable perovskite solar cells. *Science*, *356*(6334), 167-171.

36. Zhu, L., Shao, Z., Ye, J., Zhang, X., Pan, X., and Dai, S. (2016). Mesoporous BaSnO 3 layer based perovskite solar cells. *Chemical Communications*, *52*(5), 970-973.

37. Amtout, A., and Leonelli, R. (1995). Optical properties of rutile near its fundamental band gap. *Physical Review B*, *51*(11), 6842.

38. Ke, W., Fang, G., Liu, Q., Xiong, L., Qin, P., Tao, H., ... and Yan, Y. (2015). Low-temperature solution-processed tin oxide as an alternative electron transporting layer for efficient perovskite solar cells. *Journal of the American Chemical Society*, *137*(21), 6730-6733.

39. Jiang, Q., Zhao, Y., Zhang, X., Yang, X., Chen, Y., Chu, Z., ... and You, J. (2019). Surface passivation of perovskite film for efficient solar cells. *Nature Photonics*, *13*(7), 460-466.

40. Mohamad Noh, M. F., Teh, C. H., Daik, R., Lim, E. L., Yap, C. C., Ibrahim, M. A., ... and Mohd Yusoff, A. R. b.; Jang.

41. Singh, R., Sandhu, S., and Lee, J. J. (2019). Elucidating the effect of shunt losses on the performance of mesoporous perovskite solar cells. *Solar Energy*, *193*, 956-961.

42. Singh, R., Ryu, I., Yadav, H., Park, J., Jo, J. W., Yim, S., and Lee, J. J. (2019). Non-hydrolytic sol-gel route to synthesize TiO2 nanoparticles under ambient conditions for highly efficient and stable perovskite solar cells. *Solar Energy*, *185*, 307-314.

43. Savenije, T. J., Ponseca Jr, C. S., Kunneman, L., Abdellah, M., Zheng, K., Tian, Y., ... and Sundström, V. (2014). Thermally activated exciton dissociation and recombination control the carrier dynamics in organometal halide perovskite. *The journal of physical chemistry letters*, *5*(13), 2189-2194.

44. Stranks, S. D., Eperon, G. E., Grancini, G., Menelaou, C., Alcocer, M. J., Leijtens, T., ... and Snaith, H. J. (2013). Electron-hole diffusion lengths exceeding 1 micrometer in an organometal trihalide perovskite absorber. *Science*, *342*(6156), 341-344.

45. Dong, Q., Fang, Y., Shao, Y., Mulligan, P., Qiu, J., Cao, L., and Huang, J. (2015). Electron-hole diffusion lengths> 175 μm in solution-grown CH3NH3PbI3 single crystals. *Science*, *347*(6225), 967-970.

46. Wetzelaer, G. J. A., Scheepers, M., Sempere, A. M., Momblona, C., Ávila, J., and Bolink, H. J. (2015). Trap-assisted non-radiative recombination in organic–inorganic perovskite solar cells. *Advanced Materials*, *27*(11), 1837-1841.

47. Nazeeruddin, M. K., and Snaith, H. (2015). Methylammonium lead triiodide perovskite solar cells: A new paradigm in photovoltaics. *Mrs Bulletin*, *40*(8), 641-645.

48. Singh, R., Suranagi, S. R., Yang, S. J., and Cho, K. (2018). Enhancing the power conversion efficiency of perovskite solar cells via the controlled growth of perovskite nanowires. *Nano Energy*, *51*, 192-198.

49. Shin, G. S., Choi, W. G., Na, S., Ryu, S. O., and Moon, T. (2017). Rapid crystallization in ambient air for planar heterojunction perovskite solar cells. *Electronic Materials Letters*, *13*(1), 72-76.

50. You, J., Hong, Z., Yang, Y., Chen, Q., Cai, M., Song, T. B., ... and Yang, Y. (2014). Low-temperature solution-processed perovskite solar cells with high efficiency and flexibility. *ACS nano*, *8*(2), 1674-1680.

51. Jiang, Q., Zhang, L., Wang, H., Yang, X., Meng, J., Liu, H., ... and You, J. (2016). Enhanced electron extraction using SnO 2 for high-efficiency planar-structure HC (NH 2) 2 PbI 3-based perovskite solar cells. *Nature Energy*, *2*(1), 1-7.

52. Manseki, K., Splingaire, L., Schnupf, U., Sugiura, T., and Vafaei, S. (2020, April). Current Advances in the Preparation of SnO2 Electron Transport Materials for Perovskite Solar Cells. In *ASTFE Digital Library*. Begel House Inc.

53. Deng, Y., Dong, Q., Bi, C., Yuan, Y., and Huang, J. (2016). Air-stable, efficient mixed-cation perovskite solar cells with Cu electrode by scalable fabrication of active layer. *Advanced Energy Materials*, *6*(11), 1600372.

54. Brivio, F., Caetano, C., and Walsh, A. (2016). Thermodynamic origin of photoinstability in the CH3NH3Pb (I1–x Br x) 3 hybrid halide perovskite alloy. *The journal of physical chemistry letters*, *7*(6), 1083-1087.

55. Matsui, T., Seo, J. Y., Saliba, M., Zakeeruddin, S. M., and Grätzel, M. (2017). Room-Temperature Formation of Highly Crystalline Multication Perovskites for Efficient, Low-Cost Solar Cells. *Advanced materials*, *29*(15), 1606258.

56. Nazeeruddin, M. K., Kay, A., Rodicio, I., Humphry-Baker, R., Müller, E., Liska, P., ... and Grätzel, M. (1993). Conversion of light to electricity by cis-X2bis (2, 2'-bipyridyl-4, 4'-dicarboxylate) ruthenium (II) charge-transfer sensitizers (X= Cl-, Br-, I-, CN-, and SCN-) on nanocrystalline titanium dioxide electrodes. *Journal of the American Chemical Society*, *115*(14), 6382-6390.

57. Bach, U., Lupo, D., Comte, P., Moser, J. E., Weissörtel, F., Salbeck, J., ... and Grätzel, M. (1998). Solid-state dye-sensitized mesoporous TiO 2 solar cells with high photon-to-electron conversion efficiencies. *Nature*, *395*(6702), 583-585.

58. Hawash, Z., Ono, L. K., and Qi, Y. (2018). Recent Advances in Spiro-MeOTAD Hole Transport Material and Its Applications in Organic–Inorganic Halide Perovskite Solar Cells. *Advanced Materials Interfaces*, *5*(1), 1700623.

59. Salbeck, J., Yu, N., Bauer, J., Weissörtel, F., and Bestgen, H. (1997). Low molecular organic glasses for blue electroluminescence. *Synthetic Metals*, *91*(1-3), 209-215.

60. Svanstrom, S., Jacobsson, T. J., Boschloo, G., Johansson, E. M., Rensmo, H., and Cappel, U. B. (2020). Degradation mechanism of silver metal deposited on lead halide perovskites. *ACS applied materials and interfaces*, *12*(6), 7212-7221.

61. Wehrenfennig, C., Eperon, G. E., Johnston, M. B., Snaith, H. J., and Herz, L. M. (2014). High charge carrier mobilities and lifetimes in organolead trihalide perovskites. *Advanced materials*, *26*(10), 1584-1589.

62. Jiang, Q., Zhang, L., Wang, H., Yang, X., Meng, J., Liu, H., ... and You, J. (2016). Enhanced electron extraction using SnO 2 for high-efficiency planar-structure HC (NH 2) 2 PbI 3-based perovskite solar cells. *Nature Energy*, *2*(1), 1-7.

63. Dou, B., Miller, E. M., Christians, J. A., Sanehira, E. M., Klein, T. R., Barnes, F. S., ... and van Hest, M. F. (2017). High-performance flexible perovskite solar cells on ultrathin glass: implications of the TCO. *The journal of physical chemistry letters*, *8*(19), 4960-4966.

64. Li, F., Xu, M., Ma, X., Shen, L., Zhu, L., Weng, Y., ... and Chen, C. (2018). UV Treatment of Low-Temperature Processed SnO 2 Electron Transport Layers for Planar Perovskite Solar Cells. *Nanoscale research letters*, *13*(1), 1-7.

65. Chen, Q., Zhou, H., Hong, Z., Luo, S., Duan, H. S., Wang, H. H., ... and Yang, Y. (2014). Planar heterojunction perovskite solar cells via vapor-assisted solution process. *Journal of the American Chemical Society*, *136*(2), 622-625.

66. Xiao, M., Huang, F., Huang, W., Dkhissi, Y., Bach, U., Cheng, Y., and Spiccia, L. (2014). Perovskite solar cells hot paper a fast deposition-crystallization procedure for highly efficient lead iodide perovskite thin-film solar cells. *Angew. Chem. Int. Ed.*, *53*, 9898-9903.

67. Ahn, N., and Son, D. (2015). Y., Jang I.-H., Kang SM, Choi M., Park N.-G. *J. Am. Chem. Soc*, *137*, 8696.

68. Jiang, J., Yang, X., Huang, Y., Li, M., Tao, Q., Fei, M., ... and Wu, X. S. (2020). Improvement in solar cell efficiency based on the MAPbI3 films extracted by a mixed anti-solvent. *Applied Physics Letters*, *117*(20), 203901.

69. Wang, J., Fu, W., Jariwala, S., Sinha, I., Jen, A. K. Y., and Ginger, D. S. (2018). Reducing surface recombination velocities at the electrical contacts will improve perovskite photovoltaics. *ACS Energy Letters*, *4*(1), 222-227.

70. Jariwala, S., Sun, H., Adhyaksa, G. W., Lof, A., Muscarella, L. A., Ehrler, B., ... and Ginger, D. S. (2019). Local crystal misorientation influences non-radiative recombination in halide perovskites. *Joule*, *3*(12), 3048-3060.

71. Stolterfoht, M., Caprioglio, P., Wolff, C. M., Márquez, J. A., Nordmann, J., Zhang, S., ... and Neher, D. (2018). The perovskite/transport layer interfaces dominate non-radiative recombination in efficient perovskite solar cells. *arXiv preprint arXiv:1810.01333*.

72. Diekmann, J., Caprioglio, P., Rothhardt, D., Arvind, M., Unold, T., Kirchartz, T., ... and Stolterfoht, M. (2019). Pathways towards 30% efficient perovskite solar cells. *arXiv preprint arXiv:1910.07422*.

73. Yoo, J. J., Wieghold, S., Sponseller, M. C., Chua, M. R., Bertram, S. N., Hartono, N. T. P., ... and Bawendi, M. G. (2019). An interface stabilized perovskite solar cell with high stabilized efficiency and low voltage loss. *Energy and Environmental Science*, *12*(7), 2192-2199.

74. á Abdi-Jalebi, M., á Andaji-Garmaroudi, Z., á Cacovich, S., á Stavrakas, C., á Philippe, B., á Richter, J. M., ... and á Divitini, G. (2018). C. áDucati, RH áFriend, SD áStranks. *Nature*, *555*, 497.

75. Zhao, P., Kim, B. J., and Jung, H. S. (2018). Passivation in perovskite solar cells: A review. *Materials today energy*, *7*, 267-286.

76. Liu, Z., Deng, K., Hu, J., and Li, L. (2019). Coagulated SnO2 Colloids for High-Performance Planar Perovskite Solar Cells with Negligible Hysteresis and Improved Stability. *Angewandte Chemie*, *131*(33), 11621-11628.

77. Song, J., Zheng, E., Bian, J., Wang, X. F., Tian, W., Sanehira, Y., and Miyasaka, T. (2015). Low-temperature SnO 2-based electron selective contact for efficient and stable perovskite solar cells. *Journal of Materials Chemistry A*, *3*(20), 10837-10844.

78. Jariwala, S., Burke, S., Dunfield, S., Shallcross, C., Taddei, M., Wang, J., ... and Ginger, D. S. (2020). Approaching the limits of optoelectronic performance in mixed cation mixed halide perovskites by controlling surface recombination. arXiv preprint arXiv:2006.04025.

79. Baena, J. P. C., Steier, L., Tress, W., Saliba, M., Neutzner, S., Matsui, T., ... and Hagfeldt, A. (2015). Highly efficient planar perovskite solar cells through band alignment engineering. *Energy and Environmental Science*, *8*(10), 2928-2934.

80. Basumatary, P., & Agarwal, P. (2020). Photocurrent transient measurements in MAPbI 3 thin films. Journal of Materials Science: Materials in Electronics, 31, 10047-10054.

81. Nguyen, W. H., Bailie, C. D., Unger, E. L., & McGehee, M. D. (2014). Enhancing the hole-conductivity of spiro-OMeTAD without oxygen or lithium salts by using spiro (TFSI) 2 in perovskite and dye-sensitized solar cells. Journal of the American Chemical Society, 136(31), 10996-11001.

82. Kato, Y., Ono, L. K., Lee, M. V., Wang, S., Raga, S. R., & Qi, Y. (2015). Silver iodide formation in methyl ammonium lead iodide perovskite solar cells with silver top electrodes. Advanced Materials Interfaces, 2(13), 1500195.

83. Wang, S., Cabreros, A., Yang, Y., Hall, A. S., Valenzuela, S., Luo, Y., ... and Meng, Y. S. (2020). Impacts of the Hole Transport Layer Deposition Process on Buried Interfaces in Perovskite Solar Cells. *Cell Reports Physical Science*, *1*(7), 100103.

84. Wu, Z., Song, T., & Sun, B. (2017). Carbon-based materials used for perovskite solar cells. ChemNanoMat, 3(2), 75-88.

85. Bitton, S., & Tessler, N. (2021). Electron/hole blocking layers as ionic blocking layers in perovskite solar cells. Journal of Materials Chemistry C, 9(6), 1888-1894.